JGR Atmospheres

RESEARCH ARTICLE
10.1029/2025JD045965

Atmospheric Dust Transport to High-Elevation Dronning Maud Land, Antarctica, Modulated by Cyclonic Circulation, the Pacific Decadal Oscillation, and Source Emissions

K. C. Henson[1,2], V. H. L. Winton[1,3], K. R. Clem[2], R. Mulvaney[3], and M. M. Frey[3]

[1]Antarctic Research Centre, Victoria University of Wellington, Wellington, New Zealand, [2]School of Geography Environment and Earth Sciences, Victoria University of Wellington, Wellington, New Zealand, [3]British Antarctic Survey, Natural Environment Research Council (NERC), Cambridge, UK

Key Points:

- Dust deposition flux in high-elevation Dronning Maud Land, Antarctica, increased 10-fold over the last century versus the last millennium
- Dust is sourced from southern South America and Antarctica, and transport is linked to cyclonic activity and the Pacific Decadal Oscillation
- The 10-fold increase is best explained by enhanced source emissions due to rapid land use change and stronger cyclonic winds

Supporting Information:

Supporting Information may be found in the online version of this article.

Correspondence to:

V. H. L. Winton and M. M. Frey,
holly.winton@vuw.ac.nz;
maey@bas.ac.uk

Citation:

Henson, K. C., Winton, V. H. L., Clem, K. R., Mulvaney, R., & Frey, M. M. (2026). Atmospheric dust transport to high-elevation Dronning Maud Land, Antarctica, modulated by cyclonic circulation, the Pacific Decadal Oscillation, and source emissions. *Journal of Geophysical Research: Atmospheres*, *131*, e2025JD045965. https://doi.org/10.1029/2025JD045965

Received 23 NOV 2025
Accepted 19 MAY 2026

Author Contributions:

Conceptualization: V. H. L. Winton
Data curation: V. H. L. Winton
Formal analysis: K. C. Henson, V. H. L. Winton
Funding acquisition: R. Mulvaney, M. M. Frey
Investigation: K. C. Henson, V. H. L. Winton, K. R. Clem
Methodology: K. C. Henson, V. H. L. Winton, K. R. Clem, R. Mulvaney, M. M. Frey
Resources: R. Mulvaney, M. M. Frey
Software: K. C. Henson

Abstract The dependence of aeolian dust transport on atmospheric circulation patterns allows dust preserved in Antarctic ice cores to serve as a proxy for past circulation variability. Here, we investigate dust transport to high-elevation Dronning Maud Land (DML) in Antarctica through analysis of the 1300-year-old ISOL-ICE ice core dust record together with modeled dust transport to high-elevation DML and Pearson correlation analysis with atmospheric reanalysis data and climate indices. The ice core dust record reveals an abrupt increase in dust deposition and particle size from 1915 to 2017 relative to pre-1915 values. Dust flux increased 10, 5, and 3-fold for bulk (0.9–50 μm diameter particles), 0.9–10 μm, and 0.9–5 μm particles, respectively, while the volume fraction of 2–5 μm particles within the 0.9–5 μm range increased by 12%. Interannual correlations show that cyclonic activity south of South America, associated with the Pacific Decadal Oscillation (PDO), is the dominant identified mechanism by which dust is transported from southern South America to high-elevation DML, explaining 10%–36% of variability in dust deposition at the ice core site. The abrupt dust increase is best explained by enhanced dust emissions dominantly in southern South America related to rapid land use change, with some contribution from local Antarctic sources, both occurring within variability of cyclonic circulation south of South America and the PDO. These findings suggest that future dust transport to high-elevation DML will likely be strongly modulated by emissions, the PDO, and cyclonic activity in southern South America.

Plain Language Summary Reliable global atmospheric data for the past 45 years have been made possible due to the assimilation of satellite observations since 1979 along with increasing surface and upper-air observations. To gain insight into climate and weather patterns further back in time, wind-blown dust particles deposited in Antarctica can be useful proxies. This research focuses on dust deposits in the Dronning Maud Land (DML) region in Antarctica that have accumulated and froze in the ice sheets over the past 1,300 years. Around 1915, the dust record from the ice showed a sudden increase—10 times more dust and a 12% increase in the size of the dust particles. Through atmospheric model simulations and statistical analysis, we found that the dust here primarily came from southern South America, driven by cyclones northwest of the DML region triggered by a climate pattern known as the Pacific Decadal Oscillation (PDO). The sudden dust increase is best explained by changes in dust emissions in southern South America and Antarctica occurring within cyclone and PDO activity. By better understanding the history of climate change through these dust transport patterns, predictions of future climate change can be improved.

1. Introduction

The limited temporal coverage of modern atmospheric reanalysis data sets, especially over the Southern Hemisphere (1950s to-present), hinders the analysis of multi-decadal or longer climate and atmospheric circulation variability (e.g., Hersbach et al., 2020; Kobayashi et al., 2015). Current climate prediction capabilities for decadal and longer timescales remain limited as climate processes and variability on these timescales are less understood compared to shorter periods (Hurrell, 2009; Vera et al., 2010). Furthermore, climate indices, such as El Niño Southern Oscillation (ENSO; Wang et al., 2017) and the Pacific Decadal Oscillation (PDO; Mantua et al., 1997; Newman et al., 2016), have only been reliably observed using observations up to the last century, limiting the understanding of their centennial and longer-term variability (Mantua et al., 1997; Newman et al., 2016). To address these knowledge gaps, numerous studies have employed the use of natural archives such

Supervision: V. H. L. Winton, K. R. Clem
Validation: V. H. L. Winton
Visualization: K. C. Henson
Writing – original draft: K. C. Henson
Writing – review & editing:
K. C. Henson, V. H. L. Winton,
K. R. Clem, R. Mulvaney, M. M. Frey

as Antarctic ice core dust records (e.g., Koffman et al., 2014; Laluraj et al., 2020) and oxygen isotopes from fossil corals (e.g., Cobb et al., 2013; Emile-Geay et al., 2016) to investigate the longer-term behavior of these modes of climate variability. However, since these paleoclimatic records serve as proxies or indirect measurements of physical variables, there are inherent uncertainties in the different approaches to reconstruct past variables or indices. As proxies are often site-specific, it is important to first investigate the relationship between the proxy measurement and the target climate variable in the region of interest (e.g., Chen et al., 2021; Emile-Geay et al., 2016).

Antarctic ice cores provide records of deposition of long-range (>2000 km) transported dust from Southern Hemispheric continents (Delmonte et al., 2019). Evidence of long-range dust transport includes satellite and ground-based station observations of dust activity (Gassó et al., 2010; Gassó & Torres, 2019; Li et al., 2010), air parcel trajectory modeling (e.g., Laluraj et al., 2020; Neff & Bertler, 2015), and geochemical fingerprinting (e.g., Koffman et al., 2021; Wegner et al., 2012). However, interpretation of ice core dust records prior to the satellite era remains challenging given the lack of reliable climate observations and varying atmospheric circulation patterns driving long-range dust transport to different regions in Antarctica (e.g., Koffman et al., 2014; Li et al., 2010; McConnell et al., 2007). This underscores the need to characterize dust transport patterns using reliable atmospheric reanalysis data sets during the satellite era to provide a foundational understanding for interpreting longer ice core dust records.

Previous studies have investigated the provenance of dust deposited in high-elevation Dronning Maud Land (DML). Multiple lines of evidence support a southern South American origin for dust transported to DML during the Last Glacial Maximum through the Holocene (Albani et al., 2012; Bory et al., 2010; Gili et al., 2017; Neff & Bertler, 2015; Vanderstraeten et al., 2023; Wegner et al., 2012), with additional non-negligible input from local Antarctic dust sources (Delmonte et al., 2019; Wegner et al., 2012). The European Program for Ice Coring in Antarctica (EPICA) in DML or EPICA DML (EDML) ice core serves as the primary deep ice core data set in high-elevation DML on the East Antarctic Plateau (2,892 m a.s.l.; 75.0°S, 0.067°E). Between 2000 and 15000 years B.P., the dominant dust particle size in the EDML ice core dust record is measured to be 2.0–3.2 μm in diameter, indicative of long-range transport from remote dust sources (Wegner et al., 2015). Variations in the EDML particle size occurred during known climate shifts, such as from the Last Glacial Maximum to the warmer Holocene period, where a general increase in particle size from 1.7-2.8 μm to 2.0–3.2 μm is observed, suggesting atmospheric and climatic reorganization and consequent terrestrial dust source changes during this transition period (Wegner et al., 2015). Furthermore, Wegner et al. (2015) also found that dust deposition peaks during austral winter over the same time period, implying that dust transport to this area is also strongest during this season.

Dust production most relevant to long-range dust transport to DML is concentrated in the extratropical regions of South America. Patagonia has been observed as a primary dust source region due to its proximity to Antarctica and arid climate, with multiple locations with active dust production, such as Colhué Huapi (Gassó & Torres, 2019), Tierra del Fuego (Gassó et al., 2010), and the San Julian's Great Depression (Li et al., 2010). Dust from the subtropical high Puna-Altiplano deserts north of Patagonia has been noted to reach the South Atlantic (Gaiero et al., 2013) and East Antarctica (Gaiero, 2007) through the influence of the subtropical jet. Patagonian and Puna-Altiplano source regions are hypothesized to have alternated in emission strength between glacial and interglacial cycles (Delmonte et al., 2008). Other noteworthy dust sources north of Patagonia include central western Argentina (Gili et al., 2017), and the Argentine Pampean and loess regions (Gaiero, 2007), though these Pampean and loess areas are not considered modern-day Potential Source Areas (PSA) to Antarctica (Prospero et al., 2002).

Climate conditions over southern South America are conducive for dust production, largely influenced by westerly winds and the presence of the Andes mountain range. Due to orographic effects, precipitation is concentrated on the western side of the Andes, while dry conditions prevail in the rain shadow to the east (Garreaud et al., 2009; Paruelo et al., 1998), making this eastern region conducive for dust emissions. Low-level zonal wind variations contribute substantially to precipitation variability across synoptic and interannual time scales in Patagonia (Garreaud, 2007; Garreaud et al., 2013), with zonal wind positively (negatively) correlated to precipitation west (east) of the Andes (Garreaud et al., 2013). Atmospheric rivers play an important role in regional climate, contributing 42%–56% of annual precipitation along the mid to high latitude (39°S–56°S) west coast and immediately east of the Andes, while decreasing to 10% near the Atlantic coast (Viale et al., 2018). El

Niño (La Niña) conditions are associated with increased (decreased) precipitation in Argentine Patagonia during June to November (Compagnucci & Araneo, 2007). Atmospheric teleconnections associated with ENSO variability affect western Patagonia through regional circulation anomalies, such as an El Niño-related anticyclone during severe drought conditions in 2016 (Garreaud, 2018). Precipitation anomalies over Patagonia are also strongly linked to circumpolar zonal wind flow associated with the Southern Annular Mode (SAM) during summer (Garreaud et al., 2013). A recent study by Gómez-Fontealba et al. (2023) found that strong wind anomalies in southwestern Patagonia correlate strongly with SAM ($R = 0.67$–0.86) and the PDO ($R = 0.37$–0.55), with longer time averaging having higher correlations, while ENSO has no detectable association.

The dominant climate or circulation patterns driving long-range dust transport from Southern South America to Antarctica vary regionally and have not been conclusively determined for high-elevation DML, especially over the last two millennia. Koffman et al. (2014) suggest that dust transport from southern South America to West Antarctica is driven by southward migration of the circumpolar westerly wind belt, with shifts toward larger particle size distributions coinciding with positive SAM phases. Laluraj et al. (2020) showed that in-phase ENSO and PDO patterns, and the recent positive summer SAM trend are the dominant drivers of dust deposition from southern South America to coastal low-elevation DML. Spectral analysis of dust flux in coastal DML reveal periodicities of 2–7 and 20 years, consistent with ENSO and PDO periodicities, respectively (Laluraj et al., 2020; Lu et al., 2018). Additionally, an observed increase in circumpolar wind speeds related to the positive SAM trend since the 1980s is implicated as a cause for increased dust flux to East Antarctic during this period, evidenced by strong correlations ($R = 0.68$) between dust flux and the SAM index (Laluraj et al., 2014). Li et al. (2010) investigated a case study of a low-pressure (cyclonic) system over the Drake Passage in June 2006 where increased surface winds over southern South America led to increased dust transport to East Antarctica. Neff and Bertler (2015) note a significant correlation ($R = 0.41$) between southward air parcel trajectories and the Amundsen Sea Low during austral spring, indicating the importance of this regional atmospheric pattern in driving dust transport from Patagonia to Antarctica. Shi et al. (2023) observed that dust event frequency in Patagonia increased by a factor of 1.6 from 2000 to 2020, as recorded in surface synoptic observations of dust events. This increase is related to enhanced wind speeds, downslope wind frequency, air temperature, and a decrease in soil moisture in Patagonia. Consequently, increased dust transport toward East Antarctica was also observed through satellite observations of aerosol optical thickness, and enhanced westerly winds and cyclonic or anticyclonic activity are implicated as the primary transport drivers (Shi et al., 2023). Notably, enhanced Patagonian dust activity between 2000 and 2020 coincides with Antarctic Peninsula cooling (Turner et al., 2016) and South Pole warming (Clem et al., 2020), both linked to increased cyclonic circulation over the Drake Passage tied to the PDO. Increased dust activity in Patagonia was also noted between 1967 and 2017 through analysis of surface synoptic observations and satellite-derived aerosol (Gassó & Torres, 2019), which have been related to lake desiccation in the region (Gassó et al., 2010). Given the varying regional drivers of dust transport to Antarctica, investigating modern-day (1979–2017) dust transport to high-elevation DML helps establish key atmospheric circulation and climate patterns important for understanding dust transport to high-elevation DML and inferring past atmospheric circulation changes from Antarctic dust records.

In this study, we explore the use of a new ice core dust record from high-elevation DML in Antarctica as a potential proxy of large-scale atmospheric circulation variability and modes of climate variability before the satellite era (1979–2017). The ice core was drilled near the EDML ice core site as part of the Isotopic Constraints on Past Ozone Layer in Polar Ice (ISOL-ICE; Figure 1) program, and the dust record spans the last ∼1300 years (Winton et al., 2024). Since the temporal coverage of the EDML record covers 2000 B.C. and older (Wegner et al., 2015), the ISOL-ICE dust record partially fills in the gap in data coverage during the last 2000 years, including the satellite era. To infer past atmospheric variability from the dust record, the relationship between dust transport and atmospheric circulation patterns must first be quantified during the satellite era when both the ISOL-ICE record and atmospheric reanalysis data are available. The ISOL-ICE record enables long-term analysis of dust transport to high-elevation DML during the satellite era as it provides a 38-year dust record from 1979 to 2017, whereas previous studies utilize satellite observations of dust activity, which are temporally limited to the last ∼20 years.

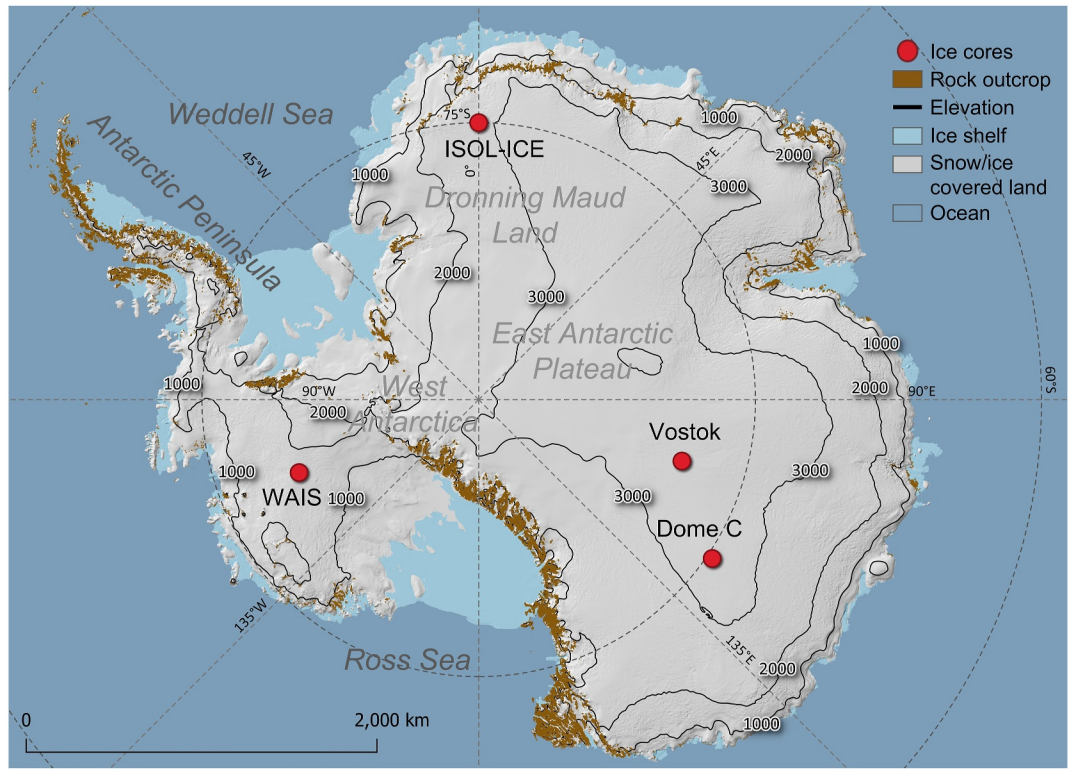

Figure 1. Map of Antarctica showing the location of ice cores mentioned in this study and relevant topographical features. Elevation is in meters above sea level. Map was generated using the Quantarctica package (Matsuoka et al., 2021). Ice cores: ISOL-ICE (Isotopic Constraints on Past Ozone Layer in Polar Ice) core at Kohnen Station, WAIS (West Antarctic Ice Sheet) Divide core, Dome C European Program for Ice Coring in Antarctica (EPICA) core, Vostok core.

2. Materials and Methods

2.1. ISOL-ICE Ice Core Dust Record

A description of the ISOL-ICE ice core, including drilling, chemical analysis, the age-depth model and the snow accumulation rate, is reported by Winton et al. (2024). The core, drilled in January 2017 at Kohnen station (74.9961°S, 0.09472°E; 2,892 m.a.s.l.) and covering the last millennium, was recovered 1 km from the deep EDML ice core site and extends the EDML record by 1300 years to the present. The high elevation of the ISOL-ICE ice core site makes the ice core record ideal for studying long-range transport of dust in the Southern Hemisphere. To date, there are limited high-resolution dust records from ice cores that include the satellite era in their temporal coverage. The ISOL-ICE ice core has the advantage of having sub-annual resolution (snow accumulation rate of 6.5 ± 2.4 cm a^{-1} w.e.) with temporal coverage up to 2017.

Here we report insoluble particle concentrations and volume size distributions (hereon referred to as particle size distributions). Insoluble particle counts were performed using a laser particle detector (Abakus, Fa.Klotz, Bad Liebenzell, Germany) which was connected to the British Antarctic Survey (BAS) continuous flow analysis system with a flow rate of 1.6 mL min^{-1} (Grieman et al., 2022). The instrument was set to measure insoluble particles in 32 individual size bins ranging between 0.9 and 50 μm. The dust mass was calculated from the measured dust particle diameter and derived volume, assuming a spherical particle density of 2.5 g cm^{-3}, and dust flux was calculated by multiplying snow accumulation rates (cm a^{-1} w.e.) with mass concentration (μg cm^{-3}). The coarse particle percentage (CPP), as a proxy for particle size, is used to determine the changes in particle size through the ice core following the approach for low-concentration Holocene dust in the EDML ice core (Wegner et al., 2015). The CPP is defined as the volume fraction of 2–5 μm particles divided by the volume fraction of 0.9–5 μm particles as described in Delmonte et al. (2004) observing a typical particle size range in East Antarctica. The same intervals were used by Lambert et al. (2008) for the high-elevation EPICA Dome C (EDC) core. Particle size distributions from selected samples are also explored using size distribution parameterized

through lognormal curve fitting as defined in Delmonte et al. (2002) to align with the curve fitting methodology used for the EDML ice core dust record (Wegner et al., 2015), enabling ease of comparison between the EDML and ISOL-ICE particle size distributions. Notably, there is uncertainty with measurements of coarse particles due to spurious counts caused by electric noise in the coulter counter technique and possible contamination of the samples (Delmonte et al., 2002). As such, many ice core studies do not focus their analyses on particles greater than 10 μm and instead use the lognormal distribution as the upper size limit (e.g., Delmonte et al., 2002; Lambert et al., 2008; McConnell et al., 2007; Wegner et al., 2015). Following this rationale from the ice core dust literature, we focus on the particles from 0.9 μm to the uppermost limit of the lognormal fit that is 10 μm for ISOL-ICE dust record (Figure S1 in Supporting Information S1).

For clarity and consistency, the following size categories are used throughout this study. Bulk or total dust (0.9–50 μm) encompasses the full measured particle size range. The 0.9–10 μm fraction represents the primary analytical range based on lognormal fitting. The 0.9–5 μm fraction includes fine particles indicative of long-range transport (Delmonte et al., 2019). Particles within 0.9–2 μm are considered very fine, while the 2–5 μm fraction represents intermediate particles. Lastly, particles greater than 10 μm represent coarse particles outside the lognormal analytical range.

To investigate the seasonality of dust deposition at the ISOL-ICE ice core site, monthly mean dust mass concentrations from 668 to 2017 CE are computed for 12 equal temporal intervals within a year to represent 12 months between mid-summer annual markers following Sommer et al. (2000) and Wegner et al. (2015). This method is adopted since the sub-annual dating of the core is based on linear interpolation between yearly austral summer sodium minima assuming that snowfall is constant throughout a year, but in reality, snow accumulation at the ISOL-ICE site is not evenly distributed throughout a year (e.g., Turner et al., 2019). In the absence of clear seasonal chemical signatures, this approach provides the best estimate for seasonal dating of particle measurements.

Spectral analysis of ice core dust concentrations and particle size is conducted using the REDFIT software (Schulz & Mudelsee, 2002) to determine key periodicities in the dust record. Both CPP and dust flux (0.9–10 μm) are used for the analysis to help filter out signals from relatively larger dust particles (>10 μm) that have likely been sourced from local Antarctic PSA. Notably, it is also possible for finer dust to originate from Antarctica, together with coarse particles. In contrast, long-range dust transport from outside Antarctica likely only includes smaller particles due to depositional processes during transport.

Given the high sampling resolution of the ISOL-ICE dust particle record (~170 particle count measurements per year), low-pass filtering using the Butterworth filter (Butterworth, 1930) is utilized to reduce noise in the dust mass concentration, flux, CPP, and snow accumulation rate data. The cutoff frequencies for the low-pass filter are 12 months (1 year) and 254 months (21 years) following Koffman et al. (2014), which featured a higher-resolution dust record from West Antarctica.

2.2. Dust Transport Modeling

The Flexpart model version 10.4 (Pisso et al., 2019) is used to run backward dust trajectories from the ISOL-ICE ice core site to determine PSAs during the satellite era. Flexpart is a Lagrangian particle dispersion model that simulates particle transport in the atmosphere. It was chosen for this study because of its dispersion modeling capabilities that allow particle size configuration, plume trajectory tracking (instead of a single particle/parcel) and emission sensitivity estimation (Pisso et al., 2019). The model is forced by meteorological fields taken from 6-hourly European Center for Medium-Range Weather Forecasts (ECMWF) Reanalysis Interim data set (ERA-Interim) with a 0.75° × 0.75° horizontal grid resolution and 60 vertical model levels (Dee et al., 2011). ERA-Interim is used instead of newer reanalysis data sets because of model compatibility reasons at the time the simulations were conducted (May-July 2021). From the ISOL-ICE ice core site, the model is configured to release a plume of 20,000 particles every 3 hr from 15 January 1979 to 31 December 2016, which is the period of temporal overlap between the ISOL-ICE dust record and ERA-Interim. Particles are then dispersed and transported backward in time for a duration of 14 days as this is the typical maximum lifetime of tropospheric particulate matter (Kok et al., 2012). The model produces back trajectories and source-receptor relationships (Seibert & Frank, 2004), also known as emission sensitivity (Pisso et al., 2019). Emission sensitivity is the average residence time of back trajectories in a given intersected grid cell and therefore describes the potential of that grid cell to contribute to particle transport to a receptor area (Pisso et al., 2019; Seibert & Frank, 2004).

A novel approach in this study is to investigate the sensitivity of the dust fetch area to particle size, seasonality, and transport height using the Flexpart model. For particle size, simulations are run using mean particle sizes of 2, 5, and 10 μm, which are based on particle size distributions in the ISOL-ICE ice core, which has a dust size mode between 3.5 and 3.7 μm over the last 1300 years (Figure S1 in Supporting Information S1; this study), and the EDML ice core, which has a 2.0–3.2 μm dust size mode over the Holocene (Wegner et al., 2015). The upper bound of 10 μm is used to capture mixed remote and local dust sources as identified at coastal ice core sites such as Roosevelt Island in Antarctica (Winton et al., 2016) due to the identification of minor local dust sources in the region (Delmonte et al., 2019). Seasonality of dust trajectories is explored by segregating the trajectories into quarterly seasons. Lastly, backward trajectories are released across four heights at the ISOL-ICE ice core site (100, 600, 1500, and 3,000 m above ground level; m.a.g.l.) to include different transport altitudes from near surface up to middle troposphere dust transport above the boundary layer (~3,000 m.a.g.l.). To determine the dominant dust transport pathways to the ISOL-ICE ice core site, trajectories are clustered using the Trajectory Statistics (TrajStat) software (Wang et al., 2009). TrajStat is a postprocessing software utilizing geographic information systems to perform various statistical analyses for simulated trajectories from trajectory models such as Flexpart. Ten-day back trajectory clusters are shown for increased readability as 14-day clusters show similar patterns with 10-day clusters except with longer trajectories.

2.3. Relationships Between Dust Deposition and Large-Scale Climate Variability

Correlation analysis was employed to investigate spatial and temporal relationships between dust deposition at the ISOL-ICE ice core site and large-scale atmospheric circulation. Specifically, Pearson correlations are computed from 1979 to 2017 for both seasonal and annual averaged data to identify persistent linear relationships between two variables. All data are detrended prior to calculating the correlations to emphasize interannual co-variability between two variables rather than spurious relationships arising from concurrent trends in the two variables. The Student's t-test is utilized for statistical significance testing where $p < 0.10$ is considered significant. We use annually averaged dust CPP (i.e., particle size) as the dust variable to represent dust deposition and transport processes (Kok et al., 2012) following Koffman et al. (2014).

Dust CPP is correlated with several atmospheric parameters from the ERA-Interim data set, including (a) meridional and zonal winds to investigate wind patterns associated with dust transport, (b) total precipitation to determine the influence of wet deposition on particle removal in the atmosphere, and (c) geopotential height to study regional and large-scale circulation patterns. ERA-Interim is used as the reanalysis data set for consistency with the dust transport modeling component of this study. Correlations between CPP and several climate indices are calculated to investigate possible connections with large-scale climate modes. The indices used in this study include the observation-based SAM index (Marshall, 2003), the Southern Oscillation Index (SOI) from the National Oceanic and Atmospheric Administration (NOAA) Climate Prediction Center, and the PDO index (Zhang et al., 1997). Supplementary correlations with additional Pacific-wide climate variables are discussed in Text S1 of Supporting Information S1.

Seasonal-mean correlations are calculated by splitting the 1979–2017 ISOL-ICE data into extended austral winter-spring (June–November) and austral summer-autumn (December–May) semesters. These groups are used for the following reasons. First, summer-autumn and winter-spring reflect extended summer and winter seasons in an environment that is influenced by sea ice variability, which generally follows these extended groupings better than traditional seasonal groupings (Stammerjohn & Maksym, 2017). Second, Crockart et al. (2021) showed that ENSO signals are most strongly preserved during winter-spring in the Mount Brown South, coastal East Antarctica (2084 m a.s.l., 69.111°S, 86.312°E), ice core record of sea salt concentrations. The seasonal correlations are derived by calculating seasonal CPP means per year and then yearly correlations are computed for each semestral grouping.

3. Results

3.1. ISOL-ICE Ice Core Dust Record

3.1.1. Dust Mass Concentration and Flux

A pronounced feature of the millennial dust deposition record is an abrupt increase in dust mass concentration, CPP, and dust flux at ~1915 CE. This timing of the abrupt increase is determined through change-point analysis

using the MATLAB algorithm findchangepts (Killick et al., 2012; Lavielle, 2005) where a significant change in mean is detected. The mean bulk (0.9–50 μm particles) dust mass concentration and dust flux during the 668–1915 CE period are ∼0.04 μg mL^{-1} (Figure 2b) and 3 mg m^{-2} yr^{-1} (Figure 2f), respectively, which then increase to 0.50 μg mL^{-1} and 30 mg m^{-2} yr^{-1}, respectively, from 1915 to 2017 CE. This translates to a ∼10-fold increase from the pre-1915 CE mean. A similar pattern is observed for 0.9–10 μm particles wherein pre-1915 CE, dust mass concentration and flux are 0.03 μg mL^{-1} (Figure 2c) and 2 mg m^{-2} yr^{-1} (Figure 2g), respectively, and increase to 0.16 μg mL^{-1} and 10 mg m^{-2} yr^{-1}, respectively, from 1915 CE to 2017 CE, translating to a ∼5x increase. For 0.9–5 μm particles, mean dust mass concentration and flux are 0.02 μg mL^{-1} (Figure 2d) and 1.12 mg m^{-2} yr^{-1} (Figure 2h) before 1915 CE, respectively, and increase to 0.06 μg mL^{-1} and 3.6 mg m^{-2} yr^{-1}, respectively, after 1915 CE, translating to a ∼3x increase. Common to bulk, 0.9–10 μm, and 0.9–5 μm particles, mass concentrations and fluxes exhibit two peaks of elevated dust concentrations in the 1930s and 2000s, with a period of relatively low values between 1940 and 1980. Before 1915 CE, the temporally variability of the three fractions is also similar, with periods of elevated deposition peaking around 700 and 1200 CE, and gradually increasing deposition from 1600 to 1915 CE, as more evident in the particle size variability (Figure 2e). In contrast, relatively weaker deposition and smaller particle size are observed around 850 and 1550 CE. These patterns indicate considerable dust deposition variability before and after 1915 CE.

Given that dust flux is computed from dust mass concentration and accumulation rate, the abrupt increase in dust flux does not appear to be related to changes in precipitation at the site as the snow accumulation rate (Figure 2i) does not show a similar sudden increase in the early-1900s CE. Instead, the accumulation rate over the entire record (668–2017 CE) shows interannual variability between 2 and 20 cm yr^{-1} (water equivalent; w.e.) with a mean of ∼6.5 cm yr^{-1} (w.e.) over the entire record (Winton et al., 2024).

Seasonal mean dust mass concentrations before and after the early-1900 abrupt increase exhibit different seasonality (Figure 3). From 668 to 1915 CE, there is a pronounced peak in August to September (winter/spring) and a broad minimum from January to July, with the lowest concentrations in June. After 1915 CE, dust mass concentrations show a broad peak with elevated values from March to September (autumn-spring), with the highest concentration in autumn. Large standard deviations were computed for the mean mass concentrations for both 668–1915 C.E. (mean: ∼0.055 μg mL^{-1}, standard deviation: 0.22–1.04 μg mL^{-1}) and 1915–2016 C.E. (mean: ∼0.56 μg mL^{-1}, standard deviation: 1.16–1.80 μg mL^{-1}), highlighting the episodic nature of dust deposition at the ISOL-ICE ice core site throughout the year. Since monthly assignments are based on linear interpolation between annual sodium minima assuming constant snowfall, the precise timing of seasonal peaks may shift within a given year. Nonetheless, the elevated winter-spring deposition before 1915 CE is consistent with dust deposition at the EDML site between ∼2000 and 15,000 years BP (Wegner et al., 2015), wherein the dust concentration maxima occurred most frequently in winter.

3.1.2. Particle Size Distribution and Coarse Particle Percentage (CPP)

The selected particle size distributions show size modes between 3.5 and 3.7 μm (Figure S1 in Supporting Information S1). Similar to Wegner et al. (2015), the high sampling resolution of the ISOL-ICE particle counts often resulted in a low total number of particles throughout the core. This precluded a robust lognormal fit for most core segments except for a few selected examples at certain depth intervals featured in Figure S1 of Supporting Information S1. Comparatively, the mode of EDML ice core dust during the Holocene (∼2000–16,000 years BP) ranged between 2.0 and 3.2 μm (Wegner et al., 2015). The mode increase from 2.0 to 3.2 μm in Holocene EDML core to 3.5–3.7 μm in the 1300-year-old ISOL-ICE core likely reflects changes in transport and/or source conditions such as enhanced wind strength. Additionally, differences in instrumental calibration of Abakus instruments during the EDML versus ISOL-ICE campaign may also contribute to the change in measured size modes.

Similar to the dust concentration and dust flux, CPP changes from a mean of 71% before 1915 CE to 83% after the abrupt shift (Figure 2e), reflecting a 12% increase in the proportion of 2–5 μm particles relative to 0.9–5 μm particles. This indicates that the increase in dust concentration and dust flux is associated with larger particles being deposited at the ISOL-ICE ice core site. Notably, there is less variance in CPP after the abrupt increase with interannual variability (12-month low-pass filtered) ranging from 60% to 90%, indicating a more consistent influx of large particles at the site from 1915 CE onwards. In contrast, CPP before 1900 CE varied between 30% and 90%.

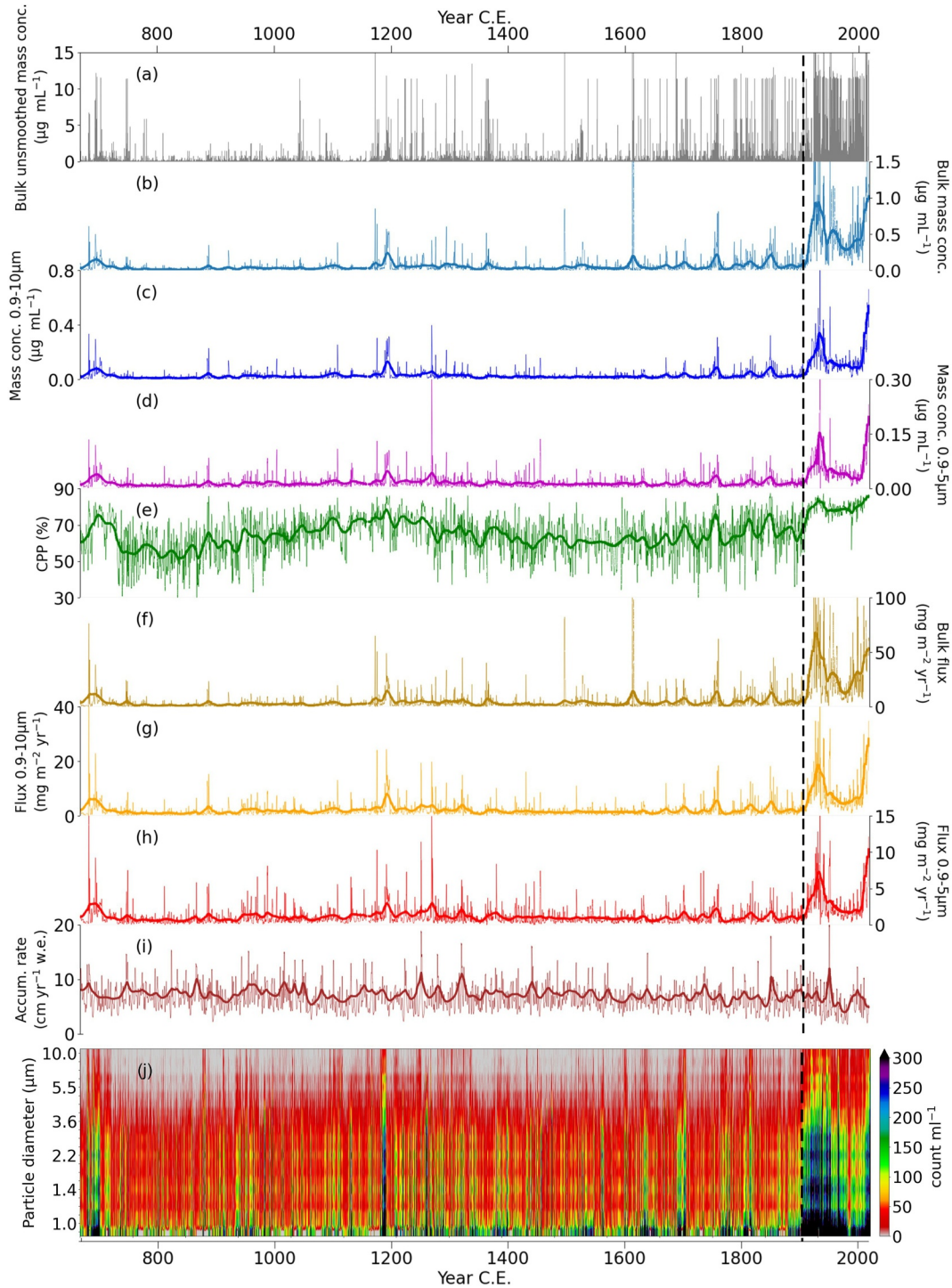

Figure 2. The ISOL-ICE ice core dust record. (a) Bulk (0.9–50 µm) unsmoothed dust mass concentration, (b) bulk dust mass concentration, (c) dust mass concentration for 0.9–10 µm particles (d) dust mass concentration for 0.9–5 µm particles, (e) coarse particle percentage (CPP), (f) bulk dust flux, (g) dust flux for 0.9–10 µm particles, (h) dust flux for 0.9–5 µm particles, (i) snow accumulation rate (water equivalent; w.e.; Winton et al., 2024), and (j) number concentration heatmap across time and particle sizes from 0.9 to 10 µm. Bold lines in panels (b–i) are low-pass filtered data with a cutoff of 12 months or 1 year (thin lines) and 254 months or 21 years (thick lines). The black vertical dashed line indicates the change point determined through change point analysis.

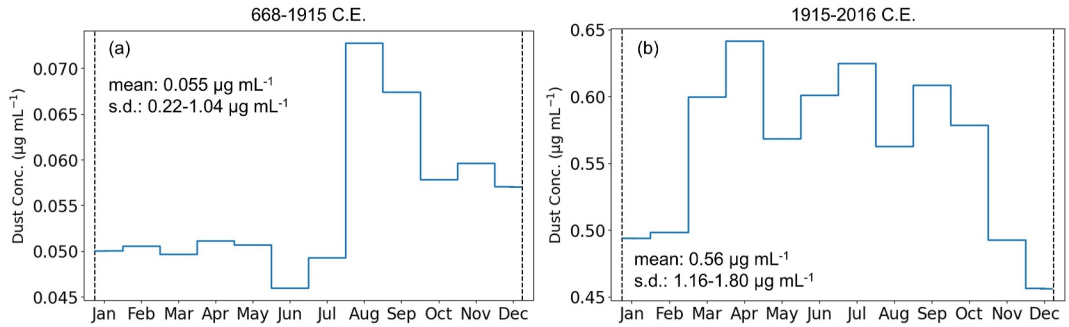

Figure 3. Mean seasonal variations in dust mass concentration for the period (a) 668–2017 CE and (b) 1915–2016 CE. Mean concentrations for each month were computed across all years. Data for each year is divided into 12 equidistant intervals corresponding to calendar months. The vertical dashed lines denote the mid-summer (December) sodium minima in the ISOL-ICE ice core.

Based on the number concentrations (Figure 2j), a shift in the size distribution and count of particles was observed starting 1915 CE. Prior to 1915 CE, most particles were less than 5 μm in size, with the greatest number concentration in the submicron range. After the 1915 CE abrupt increase, there is a shift in size distribution toward larger particles generally up to 10 μm (Figure 2j), consistent with the concurrent increase in dust CPP (Figure 2e). There is a general increase in particle count for all size bins from 0.9 to 10 μm after 1915 CE, with the largest increase in particles less than 1.2 μm in size. Notably, majority of the particles associated with the 1915 CE abrupt increase are from 0.9 to 5 μm range, with particle counts reaching up to 2500, while particles larger than 10 μm are less than 50 in number and progressively decrease with higher particle sizes. Fine 0.9–5 μm particles are therefore at least 50x more per size bin compared to particles larger than 10 μm, suggesting strong dust contribution from remote regions such as southern South America. Large particles, especially greater than 10 μm, contribute significantly to the bulk mass concentration even if fewer in number due to the size of the particles.

3.1.3. Spectral Analysis

Over the last millennium, dust deposition at the ISOL-ICE ice core site has exhibited notable periodicity. Both CPP and dust flux (0.9–10 μm) exhibit significant cycles over centennial, multi-decadal, and interannual timescales. The CPP and dust flux have centennial periodicities with frequencies of 360 and 100 years, respectively (Figures 4a and 4b). These bands are within the range of observed frequencies (∼120–400-year) for the EDC and Vostok ice core dust CPP from 9800 to 3500 years before present (Delmonte et al., 2005), strengthening evidence for possible centennial scale variability of dust deposition over the East Antarctic Plateau, though the exact drivers are still unknown. Over multi-decadal timescales, a common 17 to 20-year signal is detected in both CPP and dust flux in the ISOL-ICE dust record, and an additional 70-year band is present for CPP. Lastly, multiple significant periodicities emerge over interannual timescales ranging from 2.1 to 5.3-year cycles for both parameters with common bands at 2.6 and 4.2/4.1-year frequencies (all at >90% confidence level). For CPP, an additional 9.1-year signal is present, suggesting the presence of decadal variation as well. Notably, 20-year and 2.7 to 5-year dust flux periodicities are also observed in the coastal DML record (Laluraj et al., 2020), consistent with the observed cycles in the ISOL-ICE dust record. These interannual to multi-decadal oscillations are not resolved in the EDC and Vostok dust records due to lower temporal resolution of the ice cores (one sample every 50 years; Delmonte et al., 2005) and therefore highlight the value of high-resolution ice cores such as the ISOL-ICE record in resolving shorter-term variations, as shown in Figure 4.

Notably, the centennial-scale variations in the ISOL-ICE dust record can also be observed in the CPP timeseries (Figure 2e). Based on the 21-year filter, dust CPP reaches a minimum of 50% at 800 CE, peaks at 1200 CE with a value of 75%, and drops to another minimum of 55% at 1600 CE. This temporal pattern is also present for mass concentration and flux, albeit not as pronounced.

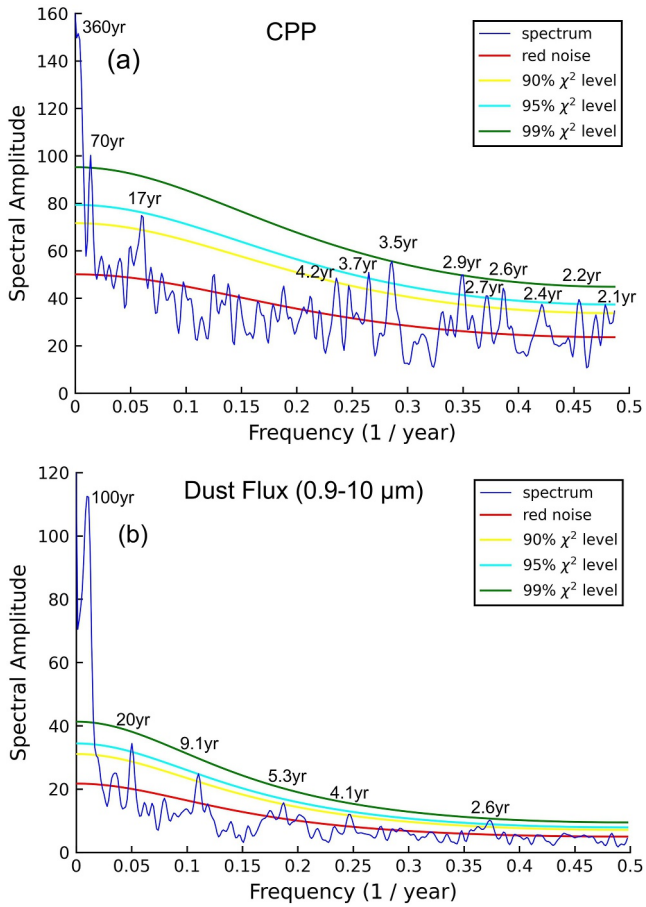

Figure 4. Spectral analysis of CPP (a) and dust flux (b) for the period 668–2017 CE. Significant periodicities ($\chi^2 > 90\%$) are labeled. Curves for red noise and confidence levels are shown.

3.2. Dust Transport Simulations

3.2.1. Emission Sensitivity

Across all the investigated particle sizes (2, 5, and 10 μm), the ISOL-ICE ice core site is most sensitive to potential dust emissions from the East Antarctic Plateau and parts of coastal DML (Figure 5a). While the emission sensitivity values are highest over the East Antarctic Plateau, this region is primarily ice covered, and hence, there are fewer potential dust sources from this area compared to sub-Antarctic landmass. However, local contribution from exposed rock surfaces near the ice core site, such as from the Heimefrontfjella mountain range near coastal DML, cannot be entirely excluded based on geochemical fingerprinting of dust in proximal ice cores tracing dust deposited at DML to local nunataks (Delmonte et al., 2019).

Among the sub-Antarctic landmasses, the highest emission sensitivity is observed over southern South America (Figure 5a). This aligns with the dominant westerly circulation, which effectively transports dust to ISOL-ICE. Based on the Flexpart simulations, within southern South America, the highest emission sensitivities for 2–5 μm particles are located along the eastern coastal region between ~47°S and 50°S (Figure 5a). South Africa, New Zealand, and south Australia show some emission sensitivity, especially for 2 μm particles, supporting secondary long-range dust contributions from South Africa (Gili et al., 2022; Vanderstraeten et al., 2023), south Australia, and New Zealand (Vanderstraeten et al., 2023).

3.2.2. Dust Trajectories

Clustering of all back trajectories from 1979 to 2017 shows various potential dust transport pathways to the ice core site (Figure 5b). The dominant clusters, collectively containing 60%–80% of trajectories, originate within westerly flow over the Southern Ocean and locally approach the ISOL-ICE ice core site from the west to the northeast. Approximately 10%–20% of trajectories arrive from the east or southeast following the local polar easterly flow. The smallest clusters, containing ~4%–8% of trajectories, follow a cross-continental flow originating from the Ross Sea region of Antarctica. Notably, none of the clusters pass over or close to the sub-Antarctic (45°S–60°S) landmass, and based on trajectory counts, trajectories originating from sub-Antarctic land areas represent less than 20% of all simulated trajectories. This suggests that most trajectories arriving at the ISOL-ICE ice core site do not originate from sub-Antarctic land areas and that long-range dust transport from sub-Antarctic regions occurs infrequently. However, while these trajectories are infrequent, they present an important contribution to dust deposition in high-elevation sites in Antarctica since sub-Antarctic landmass hosts relatively more abundant and widespread dust source areas compared to Antarctica, which is mostly ice/snow-covered (e.g., Delmonte et al., 2019; Gassó et al., 2010; Laluraj et al., 2020). Therefore, only trajectories passing over the sub-Antarctic landmass are investigated next to identify dust transport from these key sub-Antarctic PSAs.

Trajectory clusters passing over sub-Antarctic landmasses show that long-range transported dust deposited at the ISOL-ICE ice core site is primarily sourced from southern South America (Figure 5c). Across all particle sizes, at least 98% of these trajectories pass over southern South America, supporting southern South America as a PSA for long-range transported dust to the ISOL-ICE ice core site over the satellite era. The trajectory clusters originating from southern South America are all situated south of 45°S. While dry regions north of 45°S have been noted to be PSAs for dust deposited in Antarctica (Gaiero et al., 2013; Gili et al., 2017), the relative contribution of these PSAs to the high-elevation ISOL-ICE site appears to be minimal compared to PSAs south of 45°S based on our trajectory simulations given the lack of identified trajectory clusters north of 45°S. From southern South America, dust particles follow a cyclonic or clockwise flow over the South Atlantic and arrive at the ISOL-ICE ice core site from the north or northeast. A small fraction (<2%) of trajectories passing over sub-Antarctic landmasses is part of a cluster originating from New Zealand. Recent studies have also suggested South Africa as a dust source

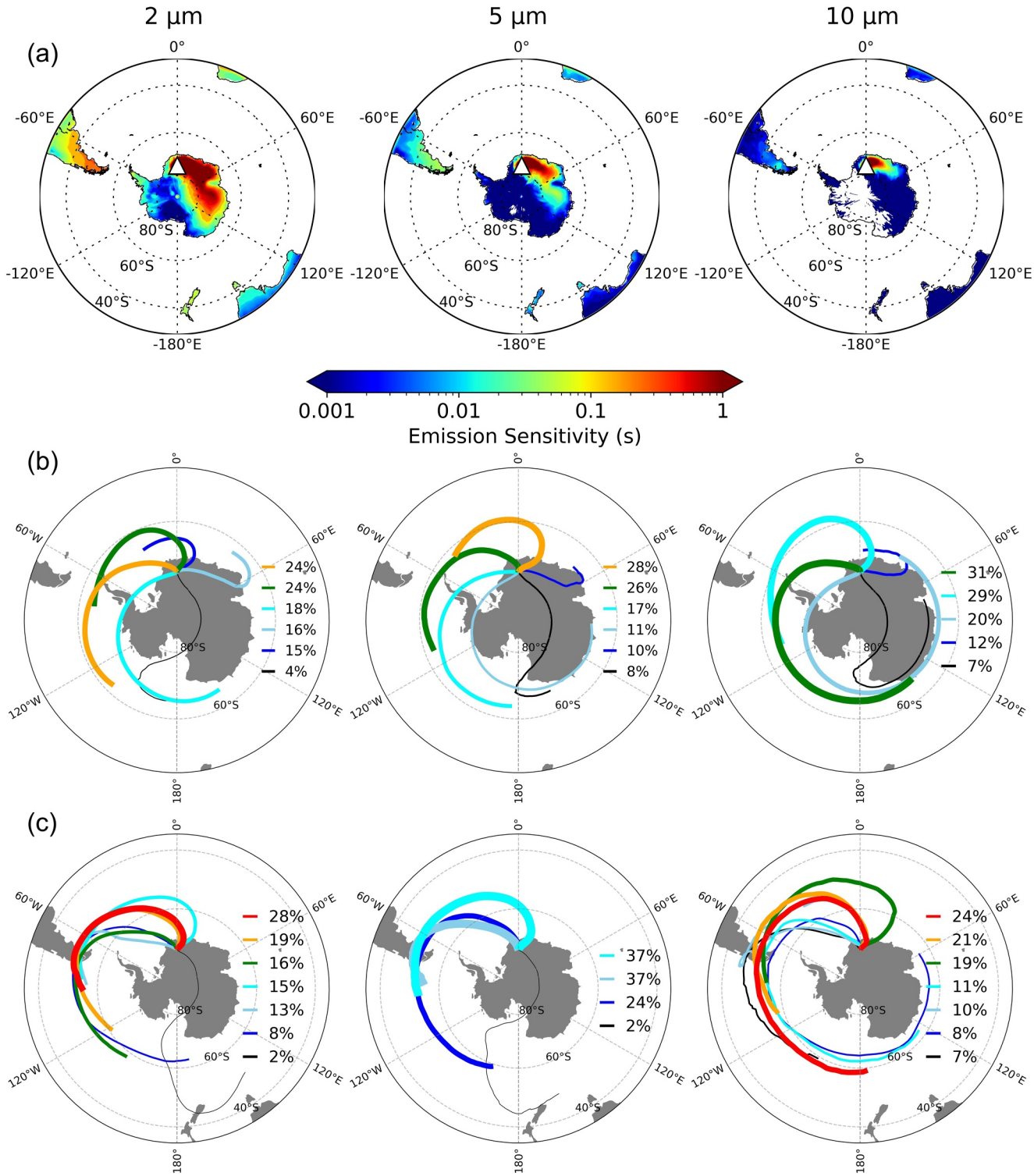

Figure 5. Emission sensitivity and 10-day back trajectory clustering across particle size (columns). (a) Average sensitivity of the ISOL-ICE ice core site (white triangle) to surface dust emissions for the period 1979–2017 for 10-day simulations. White areas on land indicate zero sensitivity. Units for emission sensitivity are in seconds, describing the residence time of back trajectories for emissions occurring in the lowest 100 m above ground level following Pisso et al. (2019). Trajectory clusters are shown for (b) all simulated trajectories and (c) trajectories passing over sub-Antarctic land areas. Trajectories are from the 1500 m.a.g.l. release height simulation. Line widths are proportional to the fraction of trajectories included in each respective cluster. Specific percentages of total trajectories included in each cluster are labeled on the right.

region for East Antarctica (Gili et al., 2022), but based on our trajectory simulations, no significant trajectory cluster was identified originating from South Africa. This indicates that southern South Africa likely contributes minimally to dust deposition at the ISOL-ICE site and only during rare dust transport events.

Based on sensitivity experiments, the horizontal component of dust trajectories from southern South America to the ISOL-ICE ice core site are generally insensitive to changes in particle size (Figures 5b and 5c), release height (i.e., transport altitude), and seasons (Figure S2 in Supporting Information S1). No systematic differences in horizontal transport routes between southern South America and high-elevation DML were observed across these parameters.

The lack of sub-Antarctic trajectory clusters identified for South Africa, New Zealand, and Australia (Figure 5c) indicates that the dominant transport pathways to the ISOL-ICE site are from southern South America. While there is emission sensitivity simulated in South Africa, New Zealand, and Australia (Figure 5a), barely any trajectory clusters or mean pathways are identified from these regions, supporting a primary southern South American origin for long-range transported dust to the ISOL-ICE site.

3.3. Relationship Between CPP and Atmospheric Circulation

3.3.1. Annual Correlations

On an annual basis, the dominant atmospheric circulation pattern associated with dust CPP variability at the ISOL-ICE ice core site is a regional circulation south of southern South America (Figure 6). Geopotential height southeast of South America exhibits a negative correlation ($R = -0.3$ to -0.4, $p < 0.1$) with dust CPP, indicating that negative pressure anomalies are associated with increased deposition of larger particles at the ISOL-ICE ice core site. This cyclonic anomaly is associated with westerly wind anomalies (positive zonal wind correlations) east of southern South America and northerly wind anomalies (negative meridional wind correlations) in the south Atlantic. Conversely, weakening of this cyclonic pattern is tied to deposition of smaller particles at the site resulting from diminished westerly and northerly winds in the mentioned regions. Notably, the wind correlations decrease with higher atmospheric levels, indicating that transport to high-elevation DML generally represents weaker (or less frequent) transport as there is stronger advection of dust particles within lower atmospheric levels. In addition, the spatial pattern of meridional wind correlations indicates that northerly wind anomalies are strongest north of the ISOL-ICE ice core site as observed in the 700 and 500 mb levels, consistent with deposition to high-elevation DML.

In addition to winds, the cyclonic system modulates precipitation over southern South America. In particular, a region of negative correlations is observed over eastern southern South America at ~50°S, with R-values ranging from −0.3 to −0.5 ($p < 0.1$). The correlations indicate that lower (higher) amounts of precipitation over eastern southern South America are associated with the deposition of larger (smaller) particles at the ISOL-ICE ice core site. Between southern South America and the ice core site, no other notable region of negative correlations is observed, suggesting that the influence of precipitation patterns is mostly constrained to the eastern southern South America region. This regional relationship can be explained by the fact that the highest dust concentrations in the entire transport pathway are typically located over source regions, and dust entrainment (influenced by soil moisture) and wet removal of particles are most strongly affected by precipitation over the southern South America region.

To determine connections between the regional circulation pattern over the Drake Passage and hemispheric-scale circulation patterns, correlation maps spanning the South Pacific and South Atlantic basins are shown in Figure S3 of Supporting Information S1. The circulation pattern over the Drake Passage appears to be tied to a Rossby wave train emanating from the central tropical Pacific near the exit region of the subtropical jet (Ding et al., 2012). The wave train is observed in both geopotential height (Figure S3a in Supporting Information S1) and stream function (Figure S3b in Supporting Information S1) correlation maps with an additional upper-level correlation cell near the equator (~170°W, 5°S) in the stream function field. The negative stream function correlations in this region (positive upper-level pressure) are associated with enhanced tropical convection, as shown in the red box in Figure S3c of Supporting Information S1. The significant negative correlation with outgoing longwave radiation indicates colder (higher) cloud tops, translating to stronger tropical convection. Convective activity in this region may therefore trigger Rossby waves that travel to the Drake Passage. The pattern is generally associated with positive SST anomalies across the central tropical Pacific resembling El Niño-like conditions, but the SST

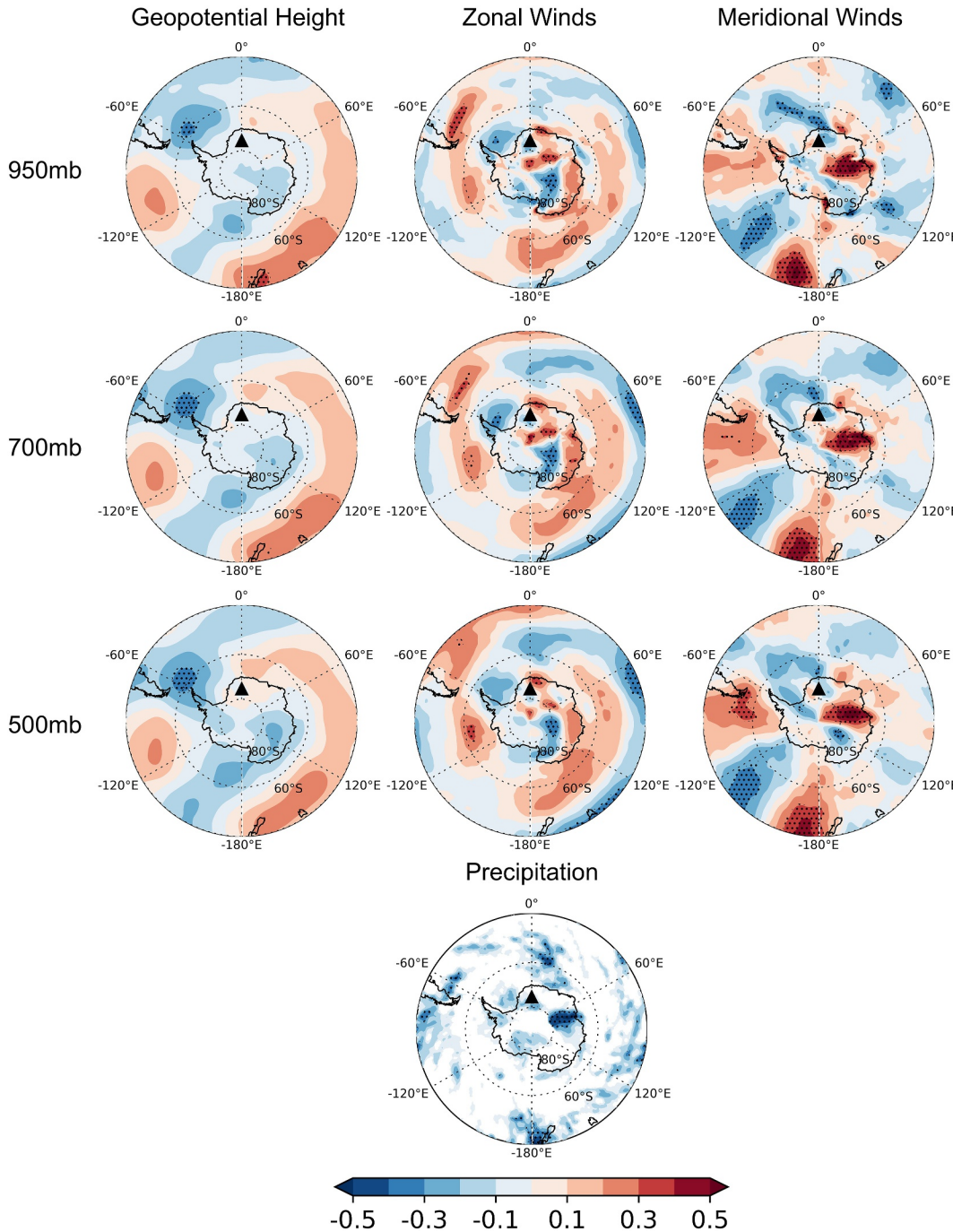

Figure 6. Correlations between annual average dust CPP at the ISOL-ICE ice core site (black triangle) and annual average geopotential height, zonal winds, meridional winds, and surface precipitation. Different atmospheric pressure levels are plotted for the first three variables to investigate changes in correlations with respect to transport level. For precipitation, only negative correlations are shown since dust transport has an inverse relationship with precipitation related to wet removal and soil moisture content. All variables were detrended prior to calculating the correlations to highlight interannual variability between parameters. Stipples denote statistical significance at $p < 0.10$.

correlations are generally weak and insignificant (Figure S3d in Supporting Information S1). Furthermore, ENSO variability is known to have a much stronger influence on circulation farther west in the Amundsen Sea region than over the Drake Passage (Li et al., 2021). Based on these correlation maps, ENSO may not be a major driver of the tropical teleconnections to the Drake Passage, and the Rossby wave pattern appears to be more tied to

localized convective variability in the central tropical Pacific. Convective variability in this region is known to be tied to a number of climate patterns, including the Madden Jullian Oscillation (Rondanelli et al., 2019), variability in the South Pacific Convergence Zone including mid-latitude wave activity (Clem et al., 2022; Matthews, 2012), and internal variability.

3.3.2. Seasonal Correlations

Seasonal correlations are investigated to determine how the relationship between CPP and large-scale atmospheric circulation may change throughout the year. Since the seasonal correlations show similar spatial patterns across pressure levels as in the annual plots, only select levels are presented in Figure 7.

During winter-spring, geopotential height correlations show a dominant negative-pressure anomaly centered west of the Antarctic Peninsula (Figure 7). The correlation values range from −0.3 to −0.5 ($p < 0.1$), and the extent and location of this pattern reflects a deepened Amundsen Sea Low (ASL). The deep ASL appears to be accompanied by a zonal wave 3 pattern across the middle latitudes, including a ridge of high pressure north of the ASL centered off the coast of Chile. The anomalous pressure gradient between these two circulation anomalies produces an anomalous westerly wind over the southeast South Pacific to southwest South Atlantic, with the highest R-values (0.4–0.6, $p < 0.1$) over the southern South America region. Northerly wind anomalies are also observed east of the Antarctic Peninsula extending from about ∼55°S to the South Pole, as indicated by the negative correlations ($R = -0.3$ to -0.4, $p < 0.1$). Notably, this region of negative correlations is west of the ice core site, indicating that southward dust transport during winter-spring occurs closer to the Antarctic Peninsula. In terms of precipitation, deepening of the ASL is associated with less precipitation over eastern coastal regions in southern South America, particularly at ∼50°S extending eastward off the coast, with correlations of $R = -0.3$ to -0.4 ($p < 0.1$).

During summer-autumn, transport of larger particles to the ice core site is associated with a low-pressure/cyclonic anomaly over the Drake Passage (Figure 7), similar to the annual correlations. Positive zonal wind correlations ($R = 0.3$–0.5, $p < 0.1$) are present east of southern South America and weak negative meridional wind correlations ($R = -0.2$ to -0.3, $p < 0.1$) over the Weddell Sea region. Despite the weak correlations, the negative meridional wind correlations still indicate anomalous northerly winds over this region favoring enhanced poleward transport of larger dust particles. Similar to winter-spring, drier conditions over the eastern coastal southern South America region (∼50°S) during summer-autumn are associated with larger particles being transported to the ice core site, with correlation values for precipitation ranging from −0.3 to −0.4 ($p < 0.1$).

Across the wider Southern Hemisphere, the winter-spring deepening of the ASL appears to be induced by a wave train originating over Australia. Both 500 mb geopotential height (Figure S4a in Supporting Information S1) and 250 mb stream function (Figure S4b in Supporting Information S1) show consistent patterns with correlation strengths between 0.3 and 0.6 ($p < 0.1$). Moreover, the low-pressure system over Australia and the high-pressure system southeast of New Zealand exhibit an elongated zonal structure with a latitudinal band of same-sign correlations extending eastward to the South Atlantic, as most clearly seen in the stream function plot. The locations and elongated structures of the pressure anomalies reflect variability in the subtropical jet, which is noted to be most pronounced and distinct from the eddy-driven polar front jet during winter (Gallego et al., 2005; Gillett et al., 2021). Notably, perturbation of the Southern Hemisphere subtropical jet is known to be related to Rossby wave propagation toward Antarctica, especially during non-summer months (e.g., Clem & Fogt, 2015; Ding et al., 2012).

The origin of the wave train appears to be linked to suppressed tropical convection northeast of Australia in the South Pacific Convergence Zone (SPCZ), shown by a diagonal band of positive correlations seen from Papua New Guinea extending south-eastward (Figure S4c in Supporting Information S1). Suppressed convective activity in the SPCZ during winter can generate an anomalous Rossby wave source along the subtropical jet, which has previously been shown to produce a cyclonic anomaly near the Antarctic Peninsula in winter (Clem et al., 2019). While studies have suggested subtropical jet variability related to ENSO activity (e.g., Ding et al., 2012; Gillett et al., 2021), the lack of significant correlations with SST over the tropical Pacific indicates that in this particular case, ENSO does not appear to be associated with this circulation pattern (Figure S4d in Supporting Information S1).

In the summer-autumn semester, the low-pressure system over the Drake Passage is part of a Rossby wave train emanating near the dateline near a local region of enhanced deep convection. The strength of the correlations for

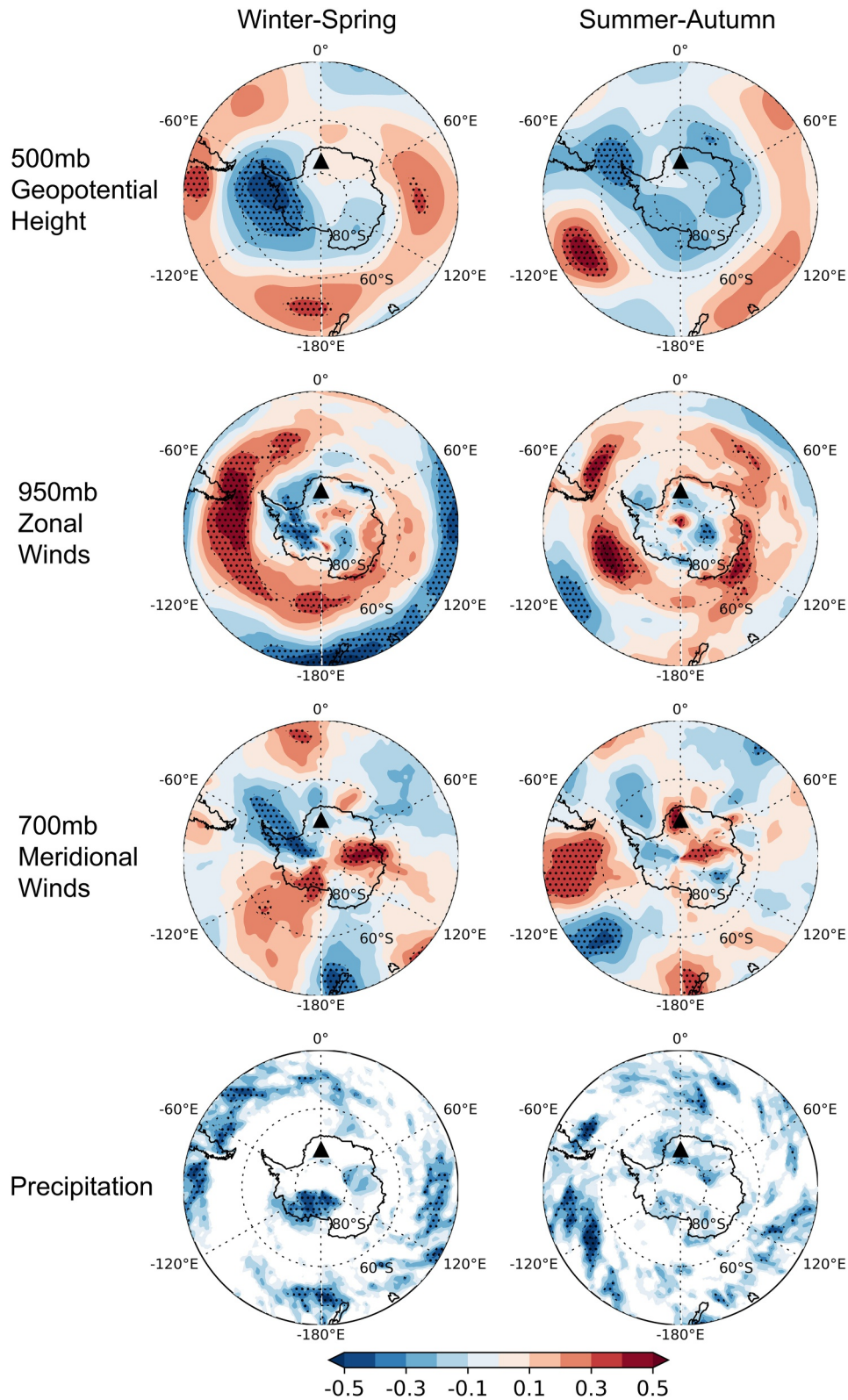

Figure 7. Same as Figure 6 but for seasonal averages and select atmospheric levels.

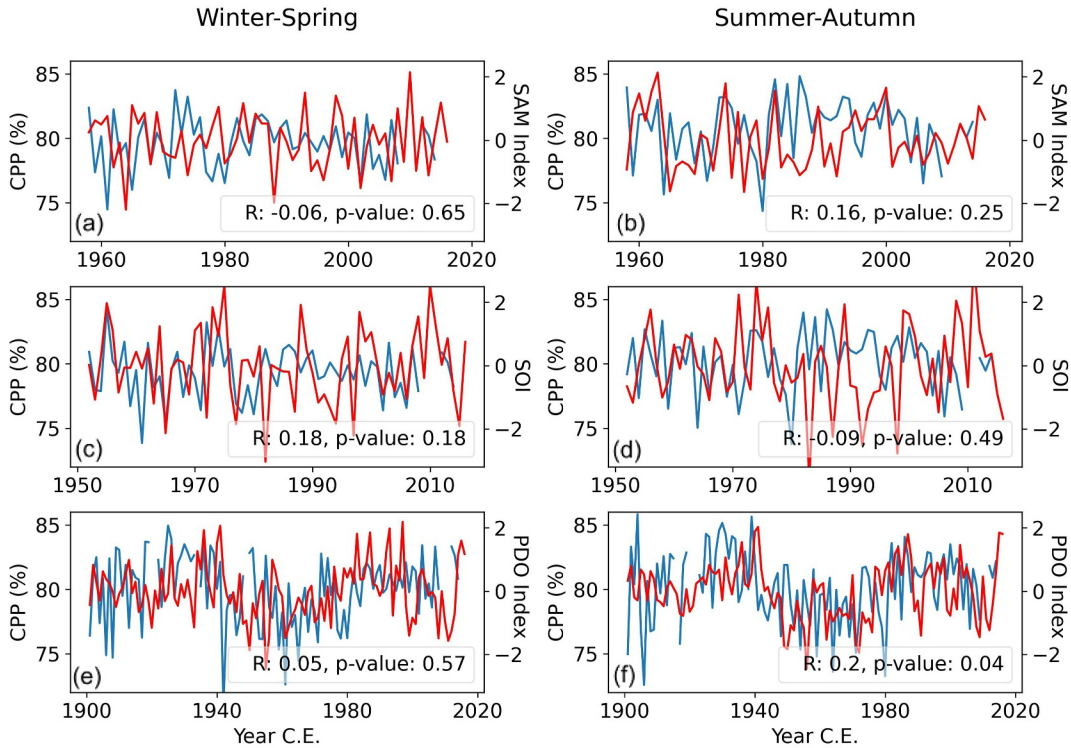

Figure 8. Winter-spring (a, c, and e) and summer-autumn (b, d, and f) average dust CPP and SAM index (a, b), SOI (c, d), and PDO index (e, f) for varying time periods. The blue line denotes dust CPP and the red line denotes the specific index. All variables are detrended to highlight interannual variability between parameters. Correlation values and statistical significance are noted at the bottom right of each plot.

both geopotential height (Figure S5a in Supporting Information S1) and stream function (Figure S5b in Supporting Information S1) ranged from 0.2 to 0.6. At ∼180°W, 20°S, the negative correlations for stream function appear to be tied to an off-equatorial band of deep convection in the SPCZ region (Figure S5c in Supporting Information S1), which again can trigger poleward wave propagation resulting in a low-pressure system over the Drake Passage during summer (Clem et al., 2019). Similar to winter-spring, dust CPP at the ice core site during summer-autumn does not have any significant correlation with SST in the tropical Pacific (Figure S5d in Supporting Information S1), thereby indicating that the discussed Rossby wave-like feature occurs largely independent of ENSO.

3.3.3. Correlations With Large-Scale Climate Patterns

Correlations between dust CPP at the ice core site and large-scale climate indices were computed to investigate potential relationships between dust transport and ENSO, SAM, or the PDO. Neither summer/autumn nor winter/spring ENSO or SAM indices show any significant correlation with dust CPP at the ice core site (Figures 8a–8d). The only significant correlation is between the PDO index and dust CPP during summer-autumn (Figure 8f). The R-value is weak ($R = 0.2$, $p < 0.1$), but the correlation is significant at the 95% confidence level, indicating a potential relationship between PDO and dust particle size at the ice core site during this period. This is consistent with previous studies linking PDO variability to anomalous circulation over the Drake Passage (Clem et al., 2019, 2020; Shi et al., 2023; Turner et al., 2016). The weak correlation value is likely due to the poor interannual (and detrended) correspondence between the PDO index and dust CPP. However, on multi-decadal time scales, there is a stronger correspondence between the PDO and CPP when considering the entire period from 1900 to 2017 (Figure 8f). Relatively high CPP is associated with positive PDO values from 1900 to 1940, both of which sharply declined in the 1940s. This is followed by a period of relatively low/negative values between the 1940 and 1980, and then increasing to a period of higher values from 1980 to 1998. Another decrease in CPP and PDO is observed from 1998 to 2010, then a sudden increase from 2010 onwards.

4. Discussion

4.1. ISOL-ICE Site Potential Source Area

The results consistently point to southern South America, south of ∼45°S, as the dominant PSA for long-range transported dust to the ISOL-ICE ice core site. Several lines of evidence support this. First, the average dust flux of 2 mg m^{-2} yr^{-1} for 0.9–10 μm particles before 1915 CE (Figure 2g) is comparable to the 1.50 mg m^{-2} yr^{-1} dust flux estimated from the EDML ice core receiving dust from remote sources in southern South America between 2,000 and 11,700 BP (Wegner et al., 2015). Second, at least 98% of Flexpart trajectories passing over sub-Antarctic land areas originate from southern South America (Figure 5c). Third, when considering only sub-Antarctic source regions, the ISOL-ICE ice core site is most sensitive to dust emissions from southern South America (Figure 5a). Lastly, the correlation maps (Figures 6 and 7) show the highest correlations in the southern South America region, suggesting an atmospheric transport connection between climatological variables in southern South America and dust deposition at the ISOL-ICE ice core site. The highest wind speed and CPP correlations are mostly from zonal wind anomalies in the southern South America region related to cyclonic circulation south of southern South America. Furthermore, negative correlations for precipitation are consistently seen in the southern South America region ∼50°S. Decreased (increased) precipitation lowers (increases) soil moisture content and interparticle cohesion, thereby making land surfaces more (less) conducive for dust emission (Kok et al., 2012).

While southern South America is the dominant PSA of long-range transported dust deposited at the ISOL-ICE ice core site, there is evidence of a non-negligible dust contribution from local Antarctic dust sources. The increase in coarse particles (>10 μm) deposited at the ice core site over the last century (Figures 2b and 2c) is indicative of contribution from nearby Antarctic dust sources, such as from the Heimefrontfjella mountain ranges in the coastal DML region as observed through radiogenic isotopes measured on dust representing the period 1700 to 1997 CE extracted from the proximal Camp Maudheimvidda ice core (73°06′19″S, 13°09′54″W; 360 m.a.s.l.; Delmonte et al., 2019). This is further supported by analysis of rare earth elements in the EDML ice core, suggesting some dust contribution from local Antarctic dust sources during the last glacial period (Wegner et al., 2012). Additionally, the highest emission sensitivities from the Flexpart simulations are also located over some parts of coastal DML (Figure 5a), supporting potential contribution from exposed rock surfaces in these areas. Local dust contribution to the East Antarctic Plateau has been noted in other studies, such as in the Zhongshan to Dome A transect where isotopic geochemical markers point to ice-free Antarctic areas as significant mineral dust sources (Du et al., 2018).

4.2. Dust Transport to the ISOL-ICE Site

Cyclonic activity south of southern South America is the dominant but non-exclusive mechanism by which dust is transported to high-elevation DMLs. This pattern is consistent with negative 500 mb geopotential height anomalies over the Bellingshausen Sea and Antarctic Peninsula associated with increased dust activity in Patagonia between 2000 and 2020 (Shi et al., 2023). Similarly, an observed dust transport event in Li et al. (2010) also linked dust transport from Patagonia to East Antarctica to a low-pressure system moving through the Drake Passage. Based on the correlation values between CPP and 500 mb geopotential height (Figures 6 and 7), the coefficient of determination (R^2) indicates that the cyclonic pattern south of southern South America explains ∼10%–36% of the dust CPP variability at the ISOL-ICE ice core site. Additional factors such as other circulation patterns, source conditions, or deposition processes may also influence interannual dust transport to the ISOL-ICE ice core site.

The negative precipitation and positive wind correlations over southern South America suggest the influence of deposition processes on dust transport. Lower (higher) amounts of precipitation lead to weakened (enhanced) wet removal of particles from the atmosphere, thereby increasing (decreasing) particle transport lifetime (Jung & Shao, 2006). Concurrently, stronger (weaker) wind speeds weaken (strengthen) gravitational settling or dry deposition, therefore increasing (decreasing) the residence time of particles in the atmosphere (Kok et al., 2012). The combined dynamics of zonal wind and precipitation variability is similarly noted in Garreaud et al. (2013), where stronger westerlies are associated with decreased precipitation east of the Andes. The spatial pattern of both precipitation and wind correlations extends from the southern South America landmass to the Atlantic Ocean to the east, indicating that the influence of depositional forces is strongest in dust source regions in southern South America and adjacent advection areas to the east. However, both wet and dry deposition also occur over the ISOL-

ICE site as influenced by onshore winds transporting moisture from the south Atlantic, resulting in precipitation over the DML plateau (Winton et al., 2024).

Cyclone-driven dust transport to Antarctica is linked to large-scale and multi-decadal PDO variability. This is evidenced by the covarying decadal trends between PDO and CPP (Figure 8f). Findings from spectral analysis also confirm a multi-decadal and interannual periodicity in dust deposition present over the last 1300 years. The 17 and 20-year signals for CPP and dust flux (Figure 4), respectively, are within PDO timescales (15–25 years; Mantua & Hare, 2002), therefore suggesting that the PDO and the cyclonic pattern south of southern South America are likely important drivers of dust deposition to the ISOL-ICE site over the past millennium. Strengthening of cyclonic activity south of South America leads to drier conditions and stronger wind flow over southern South America, thereby increasing dust emissions in the region and consequent dust transport toward DML. These results are consistent with findings in Garreaud et al. (2013) and Gómez-Fontealba et al. (2023), where westerly wind patterns and precipitation over southern South America are important for dust production and transport to Antarctica, and both production and transport are tied to large-scale climate modes.

Previous studies have reported on the association of the PDO, or its highly correlated index, the Interdecadal Pacific Oscillation, with long-range dust transport to Antarctica and other measured chemical species in ice core records. Shi et al. (2023) computed significant correlations at $R = 0.58$ between Patagonian dust frequency from September to November and PDO variability from June to August, strengthening the evidence behind a link between the PDO and dust transport from Patagonia to East Antarctica. Similar to Figure 8f in this study, low PDO/IPO index from 1940 to 1970 and high values from 1900 to 1940 and 1970 to 1990 are also observed in the reconstructed PDO indices derived from Law Dome ice core records in Vance et al. (2015, 2022) and other proxy records compiled in Henley (2017) and Porter et al. (2021). This alignment in the temporal pattern indicates that the relationship between PDO and dust transport is important over multi-decadal timescales, likely through modifying decadal variability in tropical/subtropical convection and Rossby wave activity, as seen in Figures S3–S5 of Supporting Information S1. The influence of the PDO on surface wind anomalies in Patagonia is also observed in Gómez-Fontealba et al. (2023). While the same study notes strong links to SAM as well, Figure 8 suggests the PDO as the most relevant mode for dust transport to high-elevation DML, indicating that the ENSO and SAM do not significantly influence regional circulation southeast of South America as relevant to dust transport to high-elevation DML. However, Winton et al. (2024) found significant correlations ($R = 0.26$–0.43, $p = 0.1$) between various ISOL-ICE chemical measurements (Na^+, Mg^{2+}, MSA^-, Cl^-, and SO_4^{2-}) and indices of SAM or ENSO, indicating that other modes of climate variability are important for ISOL-ICE site but not for dust transport from southern South America to the ISOL-ICE site. Notably, the PDO is also linked to variability of ENSO (Newman et al., 2016) and low-level jets (Mu et al., 2024) in South America, but no significant correlations have been identified between dust CPP at the ISOL-ICE and both the ENSO and meridional winds along the Andes, suggesting that ENSO and low-level jets do not appear to be important drivers of dust deposition variability in high-elevation DML.

Among the modeled dust transport parameters, particle size exhibits the dominant influence on dust transport from southern South America to high-elevation DML. The horizontal components of dust trajectories do not show any systematic variation across seasonality, transport height, and particle size, implying that the general horizontal dust transport pathway is insensitive to these parameters (Figure S2 in Supporting Information S1). However, the differences in emission sensitivities across particle sizes (Figure 5a) are indicative of the strong dependence of dust transport on particle size variations. This suggests that the variability in mass concentration of dust deposited at the ISOL-ICE site largely reflects a change in transported particle size from southern South America to high-elevation DML.

4.3. Implications for Dust Deposition at the ISOL-ICE Site

To help interpret the variability of the regional dust cycle in the South Atlantic Sector of Antarctica, the findings in this study over the satellite era are discussed in relation to the late Holocene ISOL-ICE and Last Glacial Maximum to early Holocene EDML ice core dust records. First, multiple lines of evidence confirm southern South America as the dominant PSA for high-elevation DML over the last glacial period through the Holocene, 15,000 to 2,000 years B.P. (Bory et al., 2010; Delmonte et al., 2019; Gili et al., 2017; Krätschmer et al., 2022; Wegner et al., 2012), and this remains unchanged even during the satellite era (Figures 5a and 5c). Second, the seasonality of dust deposition still shows strong deposition during winter-spring since the Holocene given the

common elevated winter-spring dust mass concentrations observed over the last millennium (Figure 3a) and century (Figure 3b) in the ISOL-ICE core, and during the Holocene in the EDML core (Wegner et al., 2015). The broadening of the peak deposition period from winter-spring before 1915 CE to autumn-spring after 1915 CE indicates extended dust activity throughout the year after the abrupt increase. Third, the horizontal dust trajectories and overall dust fetch area for the DML region between the last glacial period (Albani et al., 2012; Krätschmer et al., 2022) and the satellite era (Figure 5c) are still largely the same. Fourth, the snow accumulation rate at the ISOL-ICE site has been stable during the past millennium at 6.5 ± 2.4 cm a^{-1} w.e. (Winton et al., 2024). These four factors indicate that the spatial pattern of atmospheric circulation driving dust transport to the DML plateau has not significantly changed since the last glacial period.

Based on our new understanding of dust transport over the satellite era and the consistent regional dust cycle in the South Atlantic sector of Antarctica, we provide possible explanations for the early-1900 abrupt increase in dust deposition to the ISOL-ICE ice core site. The higher average dust flux of 10 mg m^{-2} yr^{-1} for 0.9–10 μm particles after 1915 CE compared to before 1915 CE (Figure 2g) could be explained by changes due to (a) increase in local dust contribution from Antarctic sources (Delmonte et al., 2019; Wegner et al., 2012), (b) strengthening atmospheric circulation and PDO variability favoring dry conditions and stronger winds that enhance atmospheric dust transport, and (c) changes in source conditions in southern South America, such as aridity and soil sediment availability related to desertification.

In terms of enhanced local dust contribution, multiple findings suggest non-negligible local dust transport to the site. The increase in CPP after 1915 (Figure 2e), the high emission sensitivities in the DML region (Figure 5a), and the Antarctic geochemical signatures from previous studies (Delmonte et al., 2019; Wegner et al., 2012), all evidence some local dust contribution from proximal ice-free surfaces, such as nunataks. This could potentially be related to stronger winds near the DML region associated with the cyclonic circulation south of South America (Figures 6 and 7). However, evidence from previous research (Albani et al., 2012; Bory et al., 2010; Gili et al., 2017; Neff & Bertler, 2015; Vanderstraeten et al., 2023; Wegner et al., 2012, 2015) and findings in this study, especially from the correlation analysis, still point to southern South America as the dominant dust source for high-elevation DML. The correlation maps in this study reveal relevant atmospheric patterns near southern South America rather than in the DML region (Figures 6 and 7). In addition, the 3.5–3.7 μm size modes in the ISOL-ICE core (Figure S1 in Supporting Information S1) are significantly smaller than the >10 μm modes observed in multiple source regions in extratropical South America, including Puna-Altiplano, the Pampas regions (Gaiero et al., 2013), San Julián, and Río Grande (Gili et al., 2017), to name a few. From 1915 onwards, the relative mass contribution of bulk particles up to 50 μm (Figure 2b) is about 6 times higher than 0.9–5 μm particles (Figure 2d), but the number concentration of fine particles smaller than 5 μm is at least 50x higher than particles larger than 10 μm (Figure 2j). Hence, relatively few coarse particles, especially greater than 10 μm, contribute significantly to bulk mass concentration due to their size, but high particle counts suggest that fine particles less than 5 μm dominate the number of particles deposited to the ISOL-ICE site. These findings indicate strong long-range transport from southern South America, with some contribution from local Antarctic dust.

Relating to circulation or modes of climate variability, while it is possible for enhanced wind speeds or drying over southern South America to increase dust emissions, there is no abrupt and persistent change in any major climate modes or atmospheric circulation that we found to be linked to dust variability at DML. PDO reconstructions do not show any concurrent abrupt increase in the early 1900s (Henley, 2017; Porter et al., 2021). Furthermore, given that the increase in DML dust concentration is not a linear change but rather a stepwise increase, we rule out the role of any long-term trends in climate, such as a positive trend in the SAM, to be the primary cause as this is inconsistent with an abrupt stepwise increase. Lastly, it is difficult to determine if there were any changes in regional atmospheric circulation due to the lack of reliable atmospheric circulation data over the Southern Ocean prior to 1979, the year when satellite-derived observations started enabling reliable global atmospheric circulation data. Thus, while not impossible, it would be speculative to suggest that the change in dust concentration is linked to atmospheric circulation changes; moreover, there would need to be a full-scale and abrupt change in atmospheric circulation to induce the stepwise change in dust concentration (rather than a long-term linear change), which is highly unlikely to have occurred and such changes have not been reported elsewhere around the Southern Hemisphere. Hence, the sudden dust increase observed in the ISOL-ICE record is likely not caused by any rapid change in PDO or cyclonic activity in the early 1900s.

Instead, we attribute the abrupt increase in dust transport to high-elevation DML to a sudden enhancement in dust source emissions dominantly in southern South America, with some contribution from local Antarctic sources. Several studies have reported major changes in land use across southern South America in the early 1900s that have increased dust emissions, including widespread overgrazing and deforestation leading to desertification (e.g., Aagesen, 2000; Bernardos et al., 2001; Del Valle et al., 1998; Viglizzo & Frank, 2006). McConnell et al. (2007) also reported significant increases in dust concentration and flux during the 1900s in a location upstream from DML at James Ross Island on the northern Antarctic Peninsula. Thus, our results are consistent with an overall increase in dust concentrations over the southern South Atlantic, likely tied to these human-induced land-use changes. In addition, the increase in CPP after 1915 (Figure 2e), high emission sensitivity over DML (Figure 5a), and geochemical signature of local Antarctic dust (Delmonte et al., 2019; Wegner et al., 2012), all evidence possible enhanced contribution from local Antarctic sources. The observed dust mass concentrations in the ISOL-ICE core after 1915 are also about 10 times higher than in other ice core dust records from low-elevation sites covering the last century (e.g., Koffman et al., 2014; Laluraj et al., 2020; McConnell et al., 2007). The ISOL-ICE core therefore records a unique dust transport signal to the high-elevation plateau that captures both enhanced long-range and local dust transport to the ISOL-ICE site. We conclude that land-use change in southern South America and local Antarctic dust contribution likely played a key role in producing the observed increase in dust concentration at high-elevation DML during the 20th century. Changes in dust emissions in these two source regions were potentially exacerbated by regional climate change favoring enhanced wind speeds and drying related to the PDO and cyclonic circulation south of South America.

A general increase in dust emissions in southern South America during the last century is supported by observations in Patagonia, revealing an increasing trend in dust activity from 1964 to 2017 associated with lake desiccation (Gassó & Torres, 2019). However, this increase in dust activity is only observed from 1964 to present as there is a lack of observation data further back in time to cover the longer ISOL-ICE dust record. Stronger dust source emissions in southern South America increase the available dust particles to be transported to high-elevation DML, explaining the higher dust deposition at the ISOL-ICE site.

In addition to the abrupt increase, the notable temporal variability between 1915 and 2017 is interpreted to be due to variability of the PDO and cyclonic activity south of South America. Three relatively high summer-autumn CPP (>80%) periods are observed during 1915–1940, 1980–1998, and 2010–2017, while a period of lower CPP (<80%) is detected during 1940–1980, and 1998–2010 (Figure 8f). The multi-decadal CPP variations follow changes in the PDO during summer-autumn (Figure 8f) that is linked to cyclonic activity south of South America (Figure 7) through Rossby wave formation (Figure S5 in Supporting Information S1). Wind and precipitation patterns associated with cyclones modulate dust transport to high-elevation DMLs. A relatively more positive summer-autumn PDO phase led to stronger cyclonic winds in southern South America and DML, coupled with reduced precipitation in southern South America, overall resulting in higher dust deposition with larger particle sizes at the ISOL-ICE site during 1915–1940, 1980–1998, and 2010–2017. Conversely, a relatively more negative summer-autumn PDO phase during 1940–1980 and 1998–2010 induced weaker cyclonic activity and enhanced precipitation leading to lower dust deposition and smaller particles at the ISOL-ICE site. The negative summer-autumn CPP-PDO period between 1998 and 2010 generally aligns with the global warming hiatus associated with negative PDO anomalies (Medhaug et al., 2017). Additionally, this variability of the PDO and cyclonic activity transported dust from source environments in southern South America and DML with already elevated dust emissions related to the abrupt increase in the early 1900s. This led to pronounced increases in dust deposition at the ISOL-ICE site during 1915–1940, 1980–1998, and 2010–2017 relative to the entire dust record.

While the summer-autumn CPP-PDO variability (Figure 8f) exhibited a decrease and increase during 1998–2010 and 2010–2017, respectively, the second abrupt increase from 1998 to 2017 in the full dust record showed a continuous upward trend (Figures 2b–2d). Based on atmospheric trend analysis, the second dust increase appears to be driven by enhanced cyclonic activity south of South America over the same period (Figure S7 in Supporting Information S1). Since the PDO exhibited negative and positive anomalies between 1998 and 2017, this enhanced cyclonic activity likely occurred in addition to PDO influence and induced westerly winds over southern South America that shift to northerlies over the South Atlantic towards high-elevation DML, consistent with Figures 6 and 7. Stronger westerly winds over southern South America and northerly winds over the South Atlantic strengthened dust transport to the ISOL-ICE site from 1998 onwards.

The association among the PDO, cyclonic circulation south of South America, and dust transport to high-elevation DML implies significant variability in the PDO and cyclonic circulation before 1915 CE based on the ISOL-ICE dust record. In particular, elevated dust deposition peaking around 700 and 1200 CE, and gradually increasing deposition and particle size from 1600 to 1915 CE at the ISOL-ICE site, both suggest heightened PDO and cyclonic activity south of South America during these periods. Consequently, stronger winds and reduced precipitation occurred in southern South America, providing more conducive conditions for dust emission and transport to high-elevation DMLs. Conversely, the minimal deposition and particle size at 850 and 1550 CE indicate weaker PDO and cyclonic activity resulting in weaker winds and increased precipitation over southern South America that reduced dust emissions and transport.

5. Summary

This study investigates dust transport to high-elevation DML in Antarctica through analysis of the 1300-year ISOL-ICE ice core dust record, Flexpart dust transport simulations, and Pearson correlation analysis with atmospheric reanalysis data and climate indices. Several analyses cover the satellite era to provide foundational work to interpret the longer ISOL-ICE dust record. The key findings are as follows:

1. Abrupt dust increase. An abrupt increase in dust deposition and particle size was observed from 1915 CE onwards relative to pre-1915 means. Dust flux increased 10-, 5-, and 3-fold for bulk (0.9–50 μm), 0.9–10 μm, and 0.9–5 μm particles, respectively, while the volume fraction of 2–5 μm particles within the 0.9–5 μm range increased by 12%. This observation has not yet been reported at other high-elevation Antarctic sites, filling a critical 1300-year gap in the nearby EDML record and enabling comparison with modern climate reanalysis data.
2. Dust source and transport mechanism. Southern South America is identified as the main dust source region for high-elevation DML from the Last Glacial Maximum through to the satellite era, with some contribution from local Antarctic sources. Cyclonic activity south of South America is the dominant identified mechanism driving dust transport, explaining 10%–36% of variability in dust deposition at the ISOL-ICE site. Enhanced cyclonic activity leads to drier conditions and increased wind flow over southern South America, creating conditions conducive for dust emission and transport toward the DML plateau. This cyclone-induced transport is linked to PDO variability through Rossby waves originating from anomalous convective activity in the tropical and subtropical Pacific, supported by spectral analysis showing multi-decadal periodicities of 17–20 years in dust CPP and flux. A novel application of the Flexpart model involving simulations across multiple particle sizes shows that horizontal dust transport pathways from southern South America to DML are generally insensitive to particle size, season, and transport height, but the strength of transport is sensitive to particle size variations.
3. Drivers of the abrupt increase. Changes in dust source location and transport pathways are ruled out based on comparison with previous research over the last glacial period and the Holocene. The abrupt increase is best explained by a sudden enhancement in dust emissions in southern South America related to rapid land use change, with some contribution from local Antarctic sources, both occurring within the variability of PDO and cyclonic activity.

Further investigation using geochemical data and extended atmospheric reanalysis data sets is needed to strengthen the analyses in this study. Geochemical fingerprinting would provide additional evidence related to dust provenance and the relative contribution of long-range transported versus local Antarctic dust. Newer reanalysis products with longer temporal coverage, such as ERA5, can be used to further support the findings on the atmospheric and climatic drivers of dust transport to high-elevation DML.

Conflict of Interest

The authors declare no conflicts of interest relevant to this study.

Availability Statement

The data sets for the ISOL-ICE dust concentration and particle size are available through the Polar Data Centre at https://doi.org/10.5285/9c972cfb-0ffa-4144-a943-da6eb82431d2 (Winton et al., 2019). ERA-Interim data were taken from Dee et al. (2011). The Flexpart model is sourced following Pisso et al. (2019), and the Trajstat software

is from Wang et al. (2009). The Quantarctica package can be downloaded from the Norwegian Polar Institute website. The SAM, PDO, and SOI data sets were obtained from Marshall (2003), Zhang et al. (1997), and the National Oceanic and Atmospheric Administration, respectively.

Acknowledgments

The ISOL-ICE ice core project was funded by a Natural Environment Research Council (NERC) Standard Grant (NE/N011813/1) to M.M.F. K.H. acknowledges support from the Antarctic Research Centre (ARC) Endowed Development Fund (Victoria University of Wellington) and the Manaaki New Zealand Scholarship. V.H.L.W. was supported by the NERC Standard Grant, and a Rutherford Foundation Postdoctoral Fellowship (RTF-VUW1801-PD) and Rutherford Discovery Fellowship (RDF-VUW2203) administrated by the Royal Society Te Apārangi. Logistics support was provided by the British Antarctic Survey (BAS), and the Alfred Wegener Institute (AWI). We would like to thank the staff from BAS and AWI for field and logistic support at Halley Station and Kohnen Station, respectively. Technical support for ice core measurements at BAS was provided by Rebecca Tuckwell, Lisa Hauge, Julius Rix, Catriona Sinclair, Emily Ludlow and Shaun Miller. We also acknowledge Dr. Benjamin Henley for sharing PDO reconstruction data and the Norwegian Polar Institute's Quantarctica package as our tool for producing detailed maps of Antarctica. Thank you for three anonymous reviewers for their constructive comments that greatly improved this manuscript. Open access publishing facilitated by Victoria University of Wellington, as part of the Wiley - Victoria University of Wellington agreement via the Council of Australasian University Librarians.

References

Aagesen, D. (2000). Crisis and conservation at the end of the world: Sheep ranching in Argentine Patagonia. *Environmental Conservation*, *27*(2), 208–215. https://doi.org/10.1017/s0376892900000229

Albani, S., Mahowald, N. M., Delmonte, B., Maggi, V., & Winckler, G. (2012). Comparing modeled and observed changes in mineral dust transport and deposition to Antarctica between the last glacial maximum and current climates. *Climate Dynamics*, *38*(9), 1731–1755. https://doi.org/10.1007/s00382-011-1139-5

Bernardos, J. N., Viglizzo, E. F., Jouvet, V., Lértora, F. A., Pordomingo, A. J., & Cid, F. D. (2001). The use of EPIC model to study the agroecological change during 93 years of farming transformation in the Argentine pampas. *Agricultural Systems*, *69*(3), 215–234. https://doi.org/10.1016/S0308-521X(01)00027-0

Bory, A., Wolff, E., Mulvaney, R., Jagoutz, E., Wegner, A., Ruth, U., & Elderfield, H. (2010). Multiple sources supply Eolian mineral dust to the Atlantic sector of coastal Antarctica: Evidence from recent snow layers at the top of Berkner Island ice sheet. *Earth and Planetary Science Letters*, *291*(1), 138–148. https://doi.org/10.1016/j.epsl.2010.01.006

Butterworth, S. (1930). On the theory of filter amplifiers. *Experimental Wireless and the Wireless Engineer*, *7*, 536–541.

Chen, C. J., Yuan, D. X., Li, J. Y., Wang, X. F., Cheng, H., Ning, Y. F., & Li, T. Y. (2021). The 4.2 ka event in East Asian monsoon region, precisely reconstructed by multi-proxies of stalagmite. *Climate of the Past Discussions*, *2021*, 1–42.

Clem, K. R., Bozkurt, D., Kennett, D., King, J. C., & Turner, J. (2022). Central tropical Pacific convection drives extreme high temperatures and surface melt on the Larsen C Ice Shelf, Antarctic Peninsula. *Nature Communications*, *13*(1), 3906. https://doi.org/10.1038/s41467-022-31119-4

Clem, K. R., & Fogt, R. L. (2015). South Pacific circulation changes and their connection to the tropics and regional Antarctic warming in austral spring, 1979–2012. *Journal of Geophysical Research: Atmospheres*, *120*(7), 2773–2792. https://doi.org/10.1002/2014JD022940

Clem, K. R., Fogt, R. L., Turner, J., Lintner, B. R., Marshall, G. J., Miller, J. R., & Renwick, J. A. (2020). Record warming at the South Pole during the past three decades. *Nature Climate Change*, *10*(8), 762–770. https://doi.org/10.1038/s41558-020-0815-z

Clem, K. R., Lintner, B. R., Broccoli, A. J., & Miller, J. R. (2019). Role of the South Pacific convergence zone in West antarctic decadal climate variability. *Geophysical Research Letters*, *46*(12), 6900–6909. https://doi.org/10.1029/2019GL082108

Cobb, K. M., Westphal, N., Sayani, H. R., Watson, J. T., Di Lorenzo, E., Cheng, H., et al. (2013). Highly variable El Niño–southern oscillation throughout the Holocene. *Science*, *339*(6115), 67–70. https://doi.org/10.1126/science.1228246

Compagnucci, R. H., & Araneo, D. C. (2007). Alcances de El Niño como predictor del caudal de los ríos andinos argentinos. *Ingeniería Hidráulica en México*, *22*(3), 23–36.

Crockart, C. K., Vance, T. R., Fraser, A. D., Abram, N. J., Criscitiello, A. S., Curran, M. A. J., et al. (2021). El Niño–Southern Oscillation signal in a new East Antarctic ice core, Mount Brown South. *Climate of the Past*, *17*(5), 1795–1818. https://doi.org/10.5194/cp-17-1795-2021

Dee, D. P., Uppala, S. M., Simmons, A. J., Berrisford, P., Poli, P., Kobayashi, S., et al. (2011). The ERA-Interim reanalysis: Configuration and performance of the data assimilation system. *Quarterly Journal of the Royal Meteorological Society*, *137*(656), 553–597. https://doi.org/10.1002/qj.828

Delmonte, B., Delmas, R. J., & Petit, J.-R. (2008). Comment on dust provenance in Antarctic ice during glacial periods: From where in southern South America? by D. M. Gaiero. *Geophysical Research Letters*, *35*(8). https://doi.org/10.1029/2007gl032075

Delmonte, B., Petit, J., & Maggi, V. (2002). Glacial to Holocene implications of the new 27000-year dust record from the EPICA Dome C (East Antarctica) ice core. *Climate Dynamics*, *18*, 647–666. https://doi.org/10.1007/s00382-001-0193-9

Delmonte, B., Petit, J. R., Andersen, K. K., Basile-Doelsch, I., Maggi, V., & Ya Lipenkov, V. (2004). Dust size evidence for opposite regional atmospheric circulation changes over East Antarctica during the last climatic transition. *Climate Dynamics*, *23*(3–4), 427–438. https://doi.org/10.1007/s00382-004-0450-9

Delmonte, B., Petit, J. R., Krinner, G., Maggi, V., Jouzel, J., & Udisti, R. (2005). Ice core evidence for secular variability and 200-year dipolar oscillations in atmospheric circulation over East Antarctica during the Holocene. *Climate Dynamics*, *24*(6), 641–654. https://doi.org/10.1007/s00382-005-0012-9

Delmonte, B., Winton, H., Baroni, M., Baccolo, G., Hansson, M., Andersson, P., et al. (2019). Holocene dust in East Antarctica: Provenance and variability in time and space. *The Holocene*, *30*(4), 546–558. https://doi.org/10.1177/0959683619875188

Del Valle, H. F., Elissalde, N. O., Gagliardini, D. A., & Milovich, J. (1998). Status of desertification in the Patagonian region: Assessment and mapping from satellite imagery. *Arid Soil Research and Rehabilitation*, *12*(2), 95–121. https://doi.org/10.1080/15324989809381502

Ding, Q., Steig, E. J., Battisti, D. S., & Wallace, J. M. (2012). Influence of the tropics on the Southern annular mode. *Journal of Climate*, *25*(18), 6330–6348. https://doi.org/10.1175/JCLI-D-11-00523.1

Du, Z., Xiao, C., Ding, M., & Li, C. (2018). Identification of multiple natural and anthropogenic sources of dust in snow from Zhongshan Station to dome A, East Antarctica. *Journal of Glaciology*, *64*(248), 855–865. https://doi.org/10.1017/jog.2018.72

Emile-Geay, J., Cobb, K. M., Carré, M., Braconnot, P., Leloup, J., Zhou, Y., et al. (2016). Links between tropical Pacific seasonal, interannual and orbital variability during the Holocene. *Nature Geoscience*, *9*(2), 168–173. https://doi.org/10.1038/ngeo2608

Gaiero, D. M. (2007). Dust provenance in Antarctic ice during glacial periods: From where in southern South America? *Geophysical Research Letters*, *34*(17). https://doi.org/10.1029/2007gl030520

Gaiero, D. M., Simonella, L., Gassó, S., Gili, S., Stein, A. F., Sosa, P., et al. (2013). Ground/satellite observations and atmospheric modeling of dust storms originating in the high puna-altiplano deserts (south America): Implications for the interpretation of paleo-climatic archives. *Journal of Geophysical Research: Atmospheres*, *118*(9), 3817–3831. https://doi.org/10.1002/jgrd.50036

Gallego, D., Ribera, P., Garcia-Herrera, R., Hernandez, E., & Gimeno, L. (2005). A new look for the Southern Hemisphere jet stream. *Climate Dynamics*, *24*(6), 607–621. https://doi.org/10.1007/s00382-005-0006-7

Garreaud, R. (2018). Record-breaking climate anomalies lead to severe drought and environmental disruption in western Patagonia in 2016. *Climate Research*, *74*(3), 217–229. https://doi.org/10.3354/cr01505

Garreaud, R., López, P., Minvielle, M., & Rojas, M. (2013). Large-scale control on the Patagonian climate. *Journal of Climate*, *26*(1), 215–230. https://doi.org/10.1175/JCLI-D-12-00001.1

Garreaud, R. D. (2007). Precipitation and circulation covariability in the extratropics. *Journal of Climate*, *20*(18), 4789–4797. https://doi.org/10.1175/JCLI4257.1

Garreaud, R. D., Vuille, M., Compagnucci, R. H., & Marengo, J. A. (2009). Present-day South American climate. *Palaeogeography, Palaeoclimatology, Palaeoecology*, *281*(3–4), 180–195. https://doi.org/10.1016/j.palaeo.2007.10.032

Gassó, S., Stein, A., Marino, F., Castellano, E., Udisti, R., & Ceratto, J. (2010). A combined observational and modeling approach to study modern dust transport from the Patagonia desert to East Antarctica. *Atmospheric Chemistry and Physics*, *10*(17), 8287–8303. https://doi.org/10.5194/acp-10-8287-2010

Gassó, S., & Torres, O. (2019). Temporal characterization of dust activity in the Central Patagonia Desert (years 1964–2017). *Journal of Geophysical Research: Atmospheres*, *124*(6), 3417–3434. https://doi.org/10.1029/2018JD030209

Gili, S., Gaiero, D. M., Goldstein, S. L., Chemale, F., Jweda, J., Kaplan, M. R., et al. (2017). Glacial/interglacial changes of Southern Hemisphere wind circulation from the geochemistry of South American dust. *Earth and Planetary Science Letters*, *469*, 98–109. https://doi.org/10.1016/j.epsl.2017.04.007

Gili, S., Vanderstraeten, A., Chaput, A., King, J., Gaiero, D. M., Delmonte, B., et al. (2022). South African dust contribution to the high southern latitudes and East Antarctica during interglacial stages. *Communications Earth & Environment*, *3*(1), 129. https://doi.org/10.1038/s43247-022-00464-z

Gillett, Z. E., Hendon, H. H., Arblaster, J. M., & Lim, E.-P. (2021). Tropical and extratropical influences on the variability of the Southern hemisphere wintertime subtropical jet. *Journal of Climate*, *34*(10), 4009–4022. https://doi.org/10.1175/JCLI-D-20-0460.1

Gómez-Fontealba, C., Flores-Aqueveque, V., & Alfaro, S. C. (2023). Teleconnection between the surface wind of western Patagonia and the Sam, Enso, and PDO modes of variability. *Atmosphere*, *14*(4), 608. https://doi.org/10.3390/atmos14040608

Grieman, M. M., Hoffmann, H. M., Humby, J. D., Mulvaney, R., Nehrbass-Ahles, C., Rix, J., et al. (2022). Continuous flow analysis methods for sodium, magnesium and calcium detection in the Skytrain ice core. *Journal of Glaciology*, *68*(267), 90–100. https://doi.org/10.1017/jog.2021.75

Henley, B. J. (2017). Pacific decadal climate variability: Indices, patterns and tropical-extratropical interactions. *Global and Planetary Change*, *155*, 42–55. https://doi.org/10.1016/j.gloplacha.2017.06.004

Hersbach, H., Bell, B., Berrisford, P., Hirahara, S., Horányi, A., Muñoz-Sabater, J., et al. (2020). The ERA5 global reanalysis. *Quarterly Journal of the Royal Meteorological Society*, *146*(730), 1999–2049. https://doi.org/10.1002/qj.3803

Hurrell, J. (2009). Decadal climate prediction: Challenges and opportunities. *IOP Conference Series: Earth and Environmental Science*, *6*(2), 022001. https://doi.org/10.1088/1755-1307/6/2/022001

Jung, E., & Shao, Y. (2006). An intercomparison of four wet deposition schemes used in dust transport modeling. *Global and Planetary Change*, *52*(1–4), 248–260. https://doi.org/10.1016/j.gloplacha.2006.02.008

Killick, R., Fearnhead, P., & Eckley, I. A. (2012). Optimal detection of changepoints with a linear computational cost. *Journal of the American Statistical Association*, *107*(500), 1590–1598. https://doi.org/10.1080/01621459.2012.737745

Kobayashi, S., Ota, Y., Harada, Y., Ebita, A., Moriya, M., Onoda, H., et al. (2015). The JRA-55 reanalysis: General specifications and basic characteristics. *Journal of the Meteorological Society of Japan. Series II*, *93*(1), 5–48. https://doi.org/10.2151/jmsj.2015-001

Koffman, B. G., Goldstein, S. L., Winckler, G., Borunda, A., Kaplan, M. R., Bolge, L., et al. (2021). New Zealand as a source of mineral dust to the atmosphere and ocean. *Quaternary Science Reviews*, *251*, 106659. https://doi.org/10.1016/j.quascirev.2020.106659

Koffman, B. G., Kreutz, K. J., Breton, D. J., Kane, E. J., Winski, D. A., Birkel, S. D., et al. (2014). Centennial-scale variability of the Southern Hemisphere westerly wind belt in the eastern Pacific over the past two millennia. *Climate of the Past*, *10*(3), 1125–1144. https://doi.org/10.5194/cp-10-1125-2014

Kok, J. F., Parteli, E. J. R., Michaels, T. I., & Karam, D. B. (2012). The physics of wind-blown sand and dust. *Reports on Progress in Physics*, *75*(10), 106901. https://doi.org/10.1088/0034-4885/75/10/106901

Krätschmer, S., van der Does, M., Lamy, F., Lohmann, G., Völker, C., & Werner, M. (2022). Simulating glacial dust changes in the Southern Hemisphere using ECHAM6.3-HAM2.3. *Climate of the Past*, *18*(1), 67–87. https://doi.org/10.5194/cp-18-67-2022

Laluraj, C. M., Rahaman, W., Thamban, M., & Srivastava, R. (2020). Enhanced dust influx to south Atlantic sector of Antarctica during the Late-20th century: Causes and contribution to radiative forcing. *Journal of Geophysical Research: Atmospheres*, *125*(8), e2019JD030675. https://doi.org/10.1029/2019JD030675

Laluraj, C. M., Thamban, M., & Satheesan, K. (2014). Dust and associated geochemical fluxes in a firn core from coastal East Antarctica and its linkages with Southern Hemisphere climate variability over the last 50 years. *Atmospheric Environment*, *90*, 23–32. https://doi.org/10.1016/j.atmosenv.2014.03.031

Lambert, F., Delmonte, B., Petit, J. R., Bigler, M., Kaufmann, P. R., Hutterli, M. A., et al. (2008). Dust-climate couplings over the past 800,000 years from the EPICA Dome C ice core. *Nature*, *452*(7187), 616–619. https://doi.org/10.1038/nature06763

Lavielle, M. (2005). Using penalized contrasts for the change-point problem. *Signal Processing*, *85*(8), 1501–1510. https://doi.org/10.1016/j.sigpro.2005.01.012

Li, F., Ginoux, P., & Ramaswamy, V. (2010). Transport of Patagonian dust to Antarctica. *Journal of Geophysical Research*, *115*(D18). https://doi.org/10.1029/2009JD012356

Li, X., Cai, W., Meehl, G. A., Chen, D., Yuan, X., Raphael, M., et al. (2021). Tropical teleconnection impacts on Antarctic climate changes. *Nature Reviews Earth & Environment*, *2*(10), 680–698. https://doi.org/10.1038/s43017-021-00204-5

Lu, B., Jin, F., & Ren, H. (2018). A coupled dynamic index for ENSO periodicity. *Journal of Climate*, *31*(6), 2361–2376. https://doi.org/10.1175/JCLI-D-17-0466.1

Mantua, N. J., & Hare, S. R. (2002). The Pacific decadal oscillation. *Journal of Oceanography*, *58*(1), 35–44. https://doi.org/10.1023/A:1015820616384

Mantua, N. J., Hare, S. R., Zhang, Y., Wallace, J. M., & Francis, R. C. (1997). A Pacific interdecadal climate oscillation with impacts on salmon production. *Bulletin of the American Meteorological Society*, *78*(6), 1069–1080. https://doi.org/10.1175/1520-0477(1997)078<1069:APICOW>2.0.CO;2

Marshall, G. J. (2003). Trends in the Southern annular mode from observations and reanalyses. *Journal of Climate*, *16*(24), 4134–4143. https://doi.org/10.1175/1520-0442(2003)016<4134:TITSAM>2.0.CO;2

Matsuoka, K., Skoglund, A., Roth, G., de Pomereu, J., Griffiths, H., Headland, R., et al. (2021). Quantarctica, an integrated mapping environment for Antarctica, the Southern Ocean, and sub-Antarctic islands. *Environmental Modelling & Software*, *140*, 105015. https://doi.org/10.1016/j.envsoft.2021.105015

Matthews, A. J. (2012). A multiscale framework for the origin and variability of the South Pacific Convergence Zone. *Quarterly Journal of the Royal Meteorological Society*, *138*(666), 1165–1178. https://doi.org/10.1002/qj.1870

McConnell, J. R., Aristarain, A. J., Banta, J. R., Edwards, P. R., & Simões, J. C. (2007). 20th-Century doubling in dust archived in an Antarctic Peninsula ice core parallels climate change and desertification in South America. *Proceedings of the National Academy of Sciences*, *104*(14), 5743–5748. https://doi.org/10.1073/pnas.0607657104

Medhaug, I., Stolpe, M. B., Fischer, E. M., & Knutti, R. (2017). Reconciling controversies about the Global Warming Hiatus. *Nature*, *545*(7652), 41–47. https://doi.org/10.1038/nature22315

Mu, Y., Jones, C., Carvalho, L. M., Xue, L., Liu, C., & Ding, Q. (2024). Pacific Decadal Oscillation and ENSO forcings of northerly low-level jets in South America. *npj Climate and Atmospheric Science*, *7*(1), 297. https://doi.org/10.1038/s41612-024-00852-6

Neff, P. D., & Bertler, N. A. N. (2015). Trajectory modeling of modern dust transport to the Southern Ocean and Antarctica. *Journal of Geophysical Research: Atmospheres*, *120*(18), 9303–9322. https://doi.org/10.1002/2015JD023304

Newman, M., Alexander, M. A., Ault, T. R., Cobb, K. M., Deser, C., Di Lorenzo, E., et al. (2016). The Pacific decadal oscillation, revisited. *Journal of Climate*, *29*(12), 4399–4427. https://doi.org/10.1175/jcli-d-15-0508.1

Paruelo, J. M., Beltrán, A., Jobbágy, E., Sala, O. E., & Golluscio, R. A. (1998). *Ecología Austral* (Vol. 8(2)). Recuperado de. Retrieved from https://bibliotecadigital.exactas.uba.ar/collection/ecologiaaustral/document/ecologiaaustral_v008_n02_p085

Pisso, I., Sollum, E., Grythe, H., Kristiansen, N. I., Cassiani, M., Eckhardt, S., et al. (2019). The Lagrangian particle dispersion model FLEXPART version 10.4. *Geoscientific Model Development*, *12*(12), 4955–4997. https://doi.org/10.5194/gmd-12-4955-2019

Porter, S. E., Mosley-Thompson, E., Thompson, L. G., & Wilson, A. B. (2021). Reconstructing an interdecadal Pacific oscillation index from a Pacific Basin–wide collection of ice core records. *Journal of Climate*, *34*(10), 3839–3852. https://doi.org/10.1175/JCLI-D-20-0455.1

Prospero, J. M., Ginoux, P., Torres, O., Nicholson, S. E., & Gill, T. E. (2002). Environmental characterization of global sources of atmospheric soil dust identified with the Nimbus 7 total ozone mapping spectrometer (TOMS) absorbing aerosol product. *Reviews of Geophysics*, *40*(1). https://doi.org/10.1029/2000rg000095

Rondanelli, R., Hatchett, B., Rutllant, J., Bozkurt, D., & Garreaud, R. (2019). Strongest MJO on record triggers extreme Atacama rainfall and warmth in Antarctica. *Geophysical Research Letters*, *46*(6), 3482–3491. https://doi.org/10.1029/2018GL081475

Schulz, M., & Mudelsee, M. (2002). REDFIT: Estimating red-noise spectra directly from unevenly spaced paleoclimatic time series. *Computers & Geosciences*, *28*(3), 421–426. https://doi.org/10.1016/s0098-3004(01)00044-9

Seibert, P., & Frank, A. (2004). Source-receptor matrix calculation with a Lagrangian particle dispersion model in backward mode. *Atmospheric Chemistry and Physics*, *4*(1), 51–63. https://doi.org/10.5194/acp-4-51-2004

Shi, C., Mao, R., Gong, D.-Y., Kim, S.-J., Feng, X., Sun, Y., & Dong, H. (2023). Increased dust transport from Patagonia to Eastern Antarctica during 2000–2020. *Global and Planetary Change*, *227*, 104186. https://doi.org/10.1016/j.gloplacha.2023.104186

Sommer, S., Wagenbach, D., Mulvaney, R., & Fischer, H. (2000). Glacio-chemical study spanning the past 2 kyr on three ice cores from Dronning Maud Land, Antarctica: 2. Seasonally resolved chemical records. *Journal of Geophysical Research*, *105*(D24), 29423–29433. https://doi.org/10.1029/2000JD900450

Stammerjohn, S., & Maksym, T. (2017). Gaining (and losing) Antarctic sea ice: Variability, trends and mechanisms. In *Sea ice*, D. N. Thomas (Ed.). https://doi.org/10.1002/9781118778371.ch10

Turner, J., Lu, H., White, I., King, J. C., Phillips, T., Hosking, J. S., et al. (2016). Absence of 21st century warming on Antarctic Peninsula consistent with natural variability. *Nature*, *535*(7612), 411–415. https://doi.org/10.1038/nature18645

Turner, J., Phillips, T., Thamban, M., Rahaman, W., Marshall, G. J., Wille, J. D., et al. (2019). The dominant role of extreme precipitation events in antarctic snowfall variability. *Geophysical Research Letters*, *46*(6), 3502–3511. https://doi.org/10.1029/2018GL081517

Vance, T. R., Kiem, A. S., Jong, L. M., Roberts, J. L., Plummer, C. T., Moy, A. D., et al. (2022). Pacific decadal variability over the last 2000 years and implications for climatic risk. *Communications Earth & Environment*, *3*(1), 33. https://doi.org/10.1038/s43247-022-00359-z

Vance, T. R., Roberts, J. L., Plummer, C. T., Kiem, A. S., & Van Ommen, T. D. (2015). Interdecadal Pacific variability and eastern Australian megadroughts over the last millennium. *Geophysical Research Letters*, *42*(1), 129–137. https://doi.org/10.1002/2014gl062447

Vanderstraeten, A., Mattielli, N., Laruelle, G. G., Gili, S., Bory, A., Gabrielli, P., et al. (2023). Identifying the provenance and quantifying the contribution of dust sources in epica dronning maud land ice core (Antarctica) over the last deglaciation (7–27 kyr BP): A high-resolution, quantitative record from a new rare earth element mixing model. *Science of The Total Environment*, *881*, 163450. https://doi.org/10.1016/j.scitotenv.2023.163450

Vera, C., Barange, M., Dube, O. P., Goddard, L., Griggs, D., Kobysheva, N., et al. (2010). Needs assessment for climate information on Decadal Timescales and longer. *Procedia Environmental Sciences*, *1*, 275–286. https://doi.org/10.1016/j.proenv.2010.09.017

Viale, M., Valenzuela, R., Garreaud, R. D., & Ralph, F. M. (2018). Impacts of atmospheric rivers on precipitation in southern South America. *Journal of Hydrometeorology*, *19*(10), 1671–1687. https://doi.org/10.1175/jhm-d-18-0006.1

Viglizzo, E. F., & Frank, F. C. (2006). Ecological interactions, feedbacks, thresholds and collapses in the Argentine Pampas in response to climate and farming during the last century. *Quaternary International*, *158*(1), 122–126. https://doi.org/10.1016/j.quaint.2006.05.022

Wang, C., Deser, C., Yu, J.-Y., DiNezio, P., & Clement, A. (2017). El niño and Southern oscillation (ENSO): A review. In *Coral reefs of the Eastern tropical Pacific persistence and loss in a dynamic environment* (1st ed.).

Wang, Y. Q., Zhang, X. Y., & Draxler, R. R. (2009). TrajStat: GIS-based software that uses various trajectory statistical analysis methods to identify potential sources from long-term air pollution measurement data. *Environmental Modelling & Software*, *24*(8), 938–939. https://doi.org/10.1016/j.envsoft.2009.01.004

Wegner, A., Fischer, H., Delmonte, B., Petit, J.-R., Erhardt, T., Ruth, U., et al. (2015). The role of seasonality of mineral dust concentration and size on glacial/interglacial dust changes in the EPICA Dronning Maud Land ice core. *Journal of Geophysical Research: Atmospheres*, *120*(19), 9916–9931. https://doi.org/10.1002/2015JD023608

Wegner, A., Gabrielli, P., Wilhelms-Dick, D., Ruth, U., Kriews, M., De Deckker, P., et al. (2012). Change in dust variability in the Atlantic sector of Antarctica at the end of the last deglaciation. *Climate of the Past*, *8*(1), 135–147. https://doi.org/10.5194/cp-8-135-2012

Winton, V. H. L., Edwards, R., Delmonte, B., Ellis, A., Andersson, P. S., Bowie, A., et al. (2016). Multiple sources of soluble atmospheric iron to Antarctic waters. *Global Biogeochemical Cycles*, *30*(3), 421–437. https://doi.org/10.1002/2015GB005265

Winton, V. H. L., Mulvaney, R., Savarino, J., Clem, K. R., & Frey, M. M. (2024). Drivers of late Holocene ice core chemistry in Dronning Maud Land: The context for the ISOL-ICE project. *Climate of the Past*, *20*(5), 1213–1232. https://doi.org/10.5194/cp-20-1213-2024

Winton, V. H. L. W., Caillon, N., Hauge, L., Mulvaney, R., Rix, J., Tuckwell, R., et al. (2019). Ice core chemistry, density, conductivity, dust, snow accumulation rate, and stable nitrate isotopic composition of the 120 m ISOL-ICE ice core, Dronning Maud Land, Antarctica (version 1.0) [Dataset]. *UK Polar Data Centre, Natural Environment Research Council, UK Research & Innovation*. https://doi.org/10.5285/9c972cfb-0ffa-4144-a943-da6eb82431d2

Zhang, Y., Wallace, J. M., & Battisti, D. S. (1997). ENSO-like interdecadal variability: 1900–93. *Journal of Climate*, *10*(5), 1004–1020. https://doi.org/10.1175/1520-0442(1997)010<1004:ELIV>2.0.CO;2

References From the Supporting Information

Huang, B., Thorne, P. W., Banzon, V. F., Boyer, T., Chepurin, G., Lawrimore, J. H., et al. (2017). Extended reconstructed sea surface temperature, version 5 (ERSSTv5): Upgrades, validations, and intercomparisons. *Journal of Climate*, *30*(20), 8179–8205. https://doi.org/10.1175/JCLI-D-16-0836.1

Lachlan-Cope, T., & Connolley, W. (2006). Teleconnections between the tropical Pacific and the Amundsen-Bellinghausens Sea: Role of the El Niño/Southern Oscillation. *Journal of Geophysical Research*, *111*(D23). https://doi.org/10.1029/2005JD006386

Liebmann, B., & Smith, C. A. (1996). Description of a complete (Interpolated) outgoing longwave radiation dataset. *Bulletin of the American Meteorological Society*, *77*(6), 1275–1277.